Seasonal differences in formation processes of oxidized organic aerosol near Houston, TX

Qili Dai[1, 2], Benjamin C. Schulze[2, 3], Xiaohui Bi[1, 2], Alexander A.T. Bui[2], Fangzhou Guo[2], Henry W. Wallace[2, 4], Nancy P. Sanchez[2], James H. Flynn[5], Barry L. Lefer[5, 6], Yinchang Feng[1*], Robert J. Griffin[2, 7]

[1] State Environmental Protection Key Laboratory of Urban Ambient Air Particulate Matter Pollution Prevention and Control, College of Environmental Science and Engineering, Nankai University, Tianjin 300350, China

[2] Department of Civil and Environmental Engineering, Rice University, Houston, TX, 77005

[3] Now at Department of Environmental Science and Engineering, California Institute of Technology, Pasadena, CA, 91125

[4] Now at Washington State Department of Ecology, Lacey WA, 98503

[5] Department of Earth and Atmospheric Sciences, University of Houston, Houston, TX, 77004

[6] Now at Division of Tropospheric Composition, NASA, Washington, DC, 20024

[7] Department of Chemical and Biomolecular Engineering, Rice University, Houston, TX, 77005

[*]Corresponding author: Yinchang Feng (fengyc@nankai.edu.cn)

Abstract

Submicron aerosol was measured to the southwest of Houston, Texas during winter and summer 2014 to investigate its seasonal variability. Data from a high-resolution time-of-flight aerosol mass spectrometer (HR-ToF-AMS) indicated that organic aerosol (OA) was the largest component of non-refractory submicron particulate matter (NR-PM_1) (on average, 38 ± 13% and 47 ± 18% of the NR-PM_1 mass loading in winter and summer, respectively). Positive matrix factorization (PMF) analysis of the OA mass spectra demonstrated that two classes of oxygenated OA (less and more-oxidized OOA, LO and MO) together dominated OA mass in summer (77%) and accounted for 39% of OA mass in winter. The fraction of LO-OOA (out of total OOA) is higher in summer (70%) than in winter (44%). Secondary aerosols (sulfate+nitrate+ammonium+OOA) accounted for ~76% and 88% of NR-PM_1 mass in winter and summer, respectively, indicating NR-PM_1 mass was driven mostly by secondary aerosol formation regardless of the season. The mass loadings and diurnal patterns of these secondary aerosols show a clear winter/summer contrast. Organic nitrate (ON) concentrations were estimated using the NO_x^+ ratio method, with contributions of 31-66% and 9-17% to OA during winter and summer, respectively. The estimated ON in summer strongly correlated with LO-OOA (r= 0.73) and was enhanced at nighttime.

The relative importance of aqueous-phase chemistry and photochemistry in processing OOA was investigated by examining the relationship of aerosol liquid water content (LWC) and the sum of ozone (O_3) and nitrogen dioxide (NO_2) (O_x=O_3+NO_2) with LO-OOA and MO-OOA. The processing mechanism of LO-OOA apparently was related to relative humidity (RH). In periods of RH <80%, aqueous-phase chemistry likely played an important role in the formation of

wintertime LO-OOA, whereas photochemistry promoted the formation of summertime LO-OOA. For periods of high RH >80%, these effects were opposite those of low RH periods. Both photochemistry and aqueous-phase processing appear to facilitate increases in MO-OOA concentration except during periods of high LWC, which is likely a result of wet removal during periods of light rain or a negative impact on its formation rate.

The nighttime increases of MO-OOA during winter and summer were 0.013 and 0.01 μg MO-OOA per μg of LWC, respectively. The increase of LO-OOA was larger than that for MO-OOA, with increase rates of 0.033 and 0.055 μg LO-OOA per μg of LWC at night during winter and summer, respectively. On average, the mass concentration of LO-OOA in summer was elevated by nearly 1.2 μg m^{-3} for a ~20 μg change in LWC, which was accompanied by a 40 ppb change in O_x.

1 Introduction

Tropospheric particulate matter (PM) has adverse effects on air quality, visibility, and ecosystems and participates in climate forcing (Watson, 2002; Grantz et al., 2003; Racherla and Adams, 2006; Tai et al., 2010; Liu et al., 2017). The various effects of PM depend on its physical, chemical and optical properties, which are determined by its emission, formation and evolution/aging processes. Atmospheric PM can either be directly emitted from primary sources (fossil fuel combustion, soil dust, sea salt, biomass burning, etc.) or formed through chemical reactions of gaseous precursors, as is the case for secondary inorganic sulfate (SO_4^{2-}) and nitrate

61 (NO_3^-) and secondary organic aerosol (SOA). Understanding the source contributions and
62 formation pathways of PM is essential for mitigating its effects (Jimenez et al., 2009).

63 Houston, TX, is of great interest to the scientific community with respect to air quality, as it
64 is the fourth most populous city in the United States (U.S.) and is well known for its energy and
65 chemical industries. Numerous efforts, from modelling (McKeen et al., 2009; Li et al., 2015;
66 Ying et al., 2015) to field measurements (for example, TexAQS 2000 and II (Bates et al., 2008;
67 Parrish et al., 2009; Atkinson et al., 2010), Go-MACCS (McKeen et al., 2009; Parrish et al.,
68 2009), TRAMP2006 (Mao et al., 2010; Cleveland et al., 2012), GC-ARCH (Allen and Fraser,
69 2006), SHARP (Olaguer et al., 2014), and DISCOVER-AQ (Bean et al., 2016; Leong et al.,
70 2017)) have been made in the Houston metropolitan area during the past two decades, providing
71 critical insights into our understanding of air quality and atmospheric chemistry with respect to
72 the sources and formation of PM. Previous field campaigns underscore that OA accounts for a
73 major fraction of non-refractory submicron PM (NR-PM_1) in Houston (Bates et al., 2008;
74 Russell et al., 2009; Cleveland et al., 2012; Brown et al., 2013; Bean et al., 2016; Leong et al.,
75 2017; Wallace et al., 2018). The spatial variation of NR-PM_1 in Houston was investigated by
76 Leong et al. (2017), who divided greater Houston into two zones based on marked differences in
77 NR-PM_1 levels, characteristics, and dynamics measured at 16 sampling locations. Zone 1 is
78 northwest of Houston and is dominated by SOA likely driven by nighttime biogenic organic
79 nitrate (ON) formation. Intensive attention has been paid recently to such
80 anthropogenic-biogenic interactions (Bahreini et al., 2009; Bean et al., 2016). Zone 2 is the
81 industrial/urban area south/east of Houston. Wallace et al. (2018) found mobile source exhaust

and petrochemical emissions likely are the most important factors impacting the NR-PM_1 and trace gases at a site in Zone 2.

Formation of SOA in clouds and the aqueous phase of aerosol particles has been reported worldwide (Lim et al., 2010; Ervens et al., 2011; Xu et al., 2017). Given that both photochemical oxidation and aqueous-phase chemistry are conducive to the formation of SOA, it is of interest to compare the relative importance of photochemistry and aqueous-phase chemistry for SOA formation in different seasons. The roles of photochemistry and aqueous-phase processing on SOA formation and evolution in different seasons in Beijing have been investigated by Hu et al. (2016) and Xu et al. (2017). Generally, aqueous-phase processing has a dominant influence on the formation of more oxidized SOA and photochemistry plays a major role in the formation of less oxidized SOA in summer and winter in Beijing, while the relative importance of these two pathways in the formation processes of SOA in autumn is different from those in summer and winter. The relative roles of aqueous-phase and photochemical processes in the formation of SOA likely vary with location and time. The seasonal differences in the spectral patterns, oxidation degrees and contributions of SOA may result from different volatile organic compound (VOC) precursors, meteorological conditions and atmospheric oxidizing capacity, which are not well understood in Houston, particularly in different seasons.

This study presents observations of NR-PM_1 from two high-resolution time-of-flight aerosol mass spectrometer (HR-ToF-AMS) measurement campaigns conducted during the winter and summer of 2014 at a site in the suburbs of Houston, where industrial and vehicular emission sources and photochemical processes are likely to play an important role in NR-PM_1 formation (Leong et al., 2017). In addition to local emissions, this site was possibly impacted by regional

marine aerosol transported from the Gulf of Mexico (Schulze et al., 2018). The aims of this work are to (1) investigate the seasonal characteristics of NR-PM_1 in the Houston area, (2) characterize the primary and secondary sources by applying positive matrix factorization (PMF) analysis to the measured OA mass spectra, and (3) evaluate the seasonal dependence of SOA composition and formation, with a main focus on the relative effects of photochemistry and aqueous-phase chemistry.

2 Materials and Methods

2.1 Sampling Site and Campaigns

Instrumentation was deployed in the University of Houston/Rice University Mobile Air Quality Laboratory (MAQL), as described in Leong et al. (2017) and Wallace et al. (2018). The winter campaign was conducted from February 3 through February 17, 2014, and the summer campaign was conducted from May 1 to May 31, 2014. The measurement site was located on the campus of University of Houston Sugar Land (UHSL) (29.5740 °N, 95.6518 °W). The campus is situated southwest of downtown and the Houston Ship Channel (HSC). The map of the measurement site is presented in Fig. S1 in the Supplemental Information (SI). The nearby interstate highway (I-69) extends to the west of downtown and serves as a major traffic emission source. The W.A. Parish Generating Station, a coal-fired power plant that is the largest electricity generating facility in Texas, is ~6 miles south of the site (Fig. S1). The data collected in the winter campaign are limited in duration; thus, the following discussion focuses primarily

on the summer campaign. The label of "winter/summer" in the text denotes the measurement period in the winter/summer.

2.2 Measurements

The data used in this paper are reported in local time, which is 6 and 5 hours behind Universal Coordinated Time in winter and summer, respectively. The details regarding the instrumental setup and data processing of these measurements were the same as described in Wallace et al. (2018). The NR-PM_1 composition was measured using an Aerodyne HR-ToF-AMS (DeCarlo et al., 2006; Canagaratna et al., 2007). A $PM_{2.5}$ Teflon®-coated cyclone inlet was installed above the MAQL at a height of 6 m above ground to remove coarse particles and to introduce air into the sampling line at a rate of 16.7 SLPM. A Nafion dryer (Perma Pure, LLC) was mounted upstream of the HR-ToF-AMS to dry the sample to below 45% relative humidity (RH). Particles are focused into a narrow beam via an aerodynamic lens and accelerated under high vacuum into the particle sizing measurement chamber. After passing the particle sizing chamber, the non-refractory components are flash vaporized at near 600^{o}C and ionized using electron impact at 70 eV. Ionized mass fragments are then transmitted directly into the time-of-flight region so that the mass spectra can be obtained. In this study, the HR-ToF-AMS was operated in "V-mode" to obtain the non-refractory chemical components with a higher sensitivity, lower mass spectral resolution compared to the "W-mode." Ionization efficiency (IE) calibration was performed monodisperse ammonium nitrate (NH_4NO_3) at the beginning and end of each campaign. Filtered ambient air was sampled every two days for approximately 20 to 30 min to provide a baseline of signal for the HR-ToF-AMS during

145 campaigns. The detection limits, (Table S1 in the SI) were calculated by multiplying the standard
146 deviations of the filter periods by three.

147 Trace gas mixing ratios and meteorological parameters also were measured on the MAQL
148 during the campaigns. Carbon monoxide (CO) was measured with high-resolution cavity
149 enhanced direct-absorption spectroscopy (Los Gatos Research, Inc.), and sulfur dioxide (SO_2)
150 was quantified using a pulsed fluorescence analyzer (ThermoFischer Scientific, model 43i-TLE).
151 Nitric oxide (NO) and nitrogen dioxide (NO_2) were measured with a chemiluminescence monitor
152 with an ultraviolet-light-emitting-diode NO_2 photolytic converter on the NO_2 channel (AQD, Inc.)
153 The total reactive nitrogen (NO_y) was measured with a Thermo 49c-TL with a heated
154 molybdenum inlet converter. Ozone (O_3) mixing ratio was measured with ultraviolet absorption
155 (2BTech, Inc., model 205). Meteorological parameters including ambient temperature, solar
156 radiation, RH, wind speed (WS), and wind direction (WD) were measured using an RM Young
157 meteorological station. Precipitation totals from a nearby Texas Commission on Environmental
158 Quality (TCEQ) monitor site (EPA Site: 48_157_0696) were downloaded from the TCEQ
159 website. The total cloud cover data were downloaded from the READY Archived Meteorology
160 website of the National Oceanic and Atmospheric Administration.

161

162 **2.3 Data Processing**

163 The HR-ToF-AMS data analysis was performed using SQUIRREL v.1.56A and PIKA
164 v.1.19D in Igor Pro 6.37 (Wave Metrics Inc.). The relative IEs were applied to OA (1.4), SO_4^{2-}
165 (1.2), NO_3^- (1.1), NH_4^+ (4.0), and chloride (Cl^-, 1.3) following the standard data analysis

166 procedures. The composition-dependent collection efficiency was applied to the data based on
167 Middlebrook et al. (2012). Elemental ratios (H/C, O/C and N/C, where H is hydrogen, C is
168 carbon, and N is nitrogen) and the ratio of organic mass to organic carbon (OM/OC) were
169 generated using the procedures described by Canagaratna et al. (2015). Example data are shown
170 in Figure S2.

171 **2.3.1 Quantification of the contributions of ON**

172 The mass loading of NO_3^- measured by HR-ToF-AMS includes both organic and inorganic
173 NO_3^-. The fragmentation ratio of NO_2^+ to NO^+ (NO_x^+ ratio) is different for ON and inorganic
174 NO_3^- (Farmer et al., 2010; Fry et al., 2013), and the NO_2^+ and NO^+ mass loadings for ON
175 ($NO_{2,ON}$ and NO_{ON}) can be estimated using the method proposed by Farmer et al. (2010):

176 $$NO_{2,ON} = \frac{NO_{2,obs} \times (R_{obs} - R_{NO_3NH_4})}{R_{ON} - R_{NO_3NH_4}} \quad (1)$$

177 $$NO_{ON} = NO_{2,ON} / R_{ON} \quad (2)$$

178 where R_{obs} is the ambient NO_x^+ ratio (0.531 and 0.260 for the winter and summer campaign,
179 respectively; see Fig. S3 for details). $R_{NO_3NH_4}$(NO_x^+ ratio of NH_4NO_3) is determined by IE
180 calibration using monodisperse NH_4NO_3 before and after the campaigns. The average of the two
181 IE calibrations was used as the $R_{NO_3NH_4}$ for the campaign (0.588 and 0.381 for the winter and
182 summer campaigns, respectively), which is comparable with the value reported elsewhere (Xu et
183 al., 2015; Zhu et al., 2016). The value of R_{ON} is hard to determine because it varies with
184 instruments and precursor VOCs (Fry et al., 2013). Previous studies found that isoprene was the
185 main biogenic VOC (BVOC) in Houston (Leuchner and Rappengluck, 2010; Kota et al., 2014),
186 and Brown et al. (2013) reported that monoterpenes and isoprene were frequently present within

187 the nocturnal boundary layer in the Houston area and underwent rapid oxidation, mainly by nitrate
188 radical (denoted as $NO_3^{\cdot}$ with a dot to differentiate it from aerosol NO_3^-). Given the abundance of
189 monoterpene and isoprene in the Houston area, similar to Xu et al. (2015), we assume organic
190 nitrates formed via isoprene and beta-pinene oxidation are representative. Fry et al. (2013)
191 assumed that the $R_{ON}/R_{NH_4NO_3}$ value is instrument-independent, and further estimated the
192 average $R_{ON}/R_{NH_4NO_3}$ of 2.25 for the organic nitrate standards. The $R_{ON}/R_{NH_4NO_3}$ values vary
193 with precursor VOC. We utilized the $R_{ON}/R_{NH_4NO_3}$ of isoprene (2.08, (Bruns et al., 2010)) and
194 beta-pinene organic nitrates (3.99, (Boyd et al., 2015)) from the literature to obtain an estimation
195 range of R_{ON} by using the NO_x^+ method.

196 The measured NO_x^+ ratio can be used to separately quantify ammonium and organic nitrates
197 as:

198 $$ON_{frac} = \frac{(R_{obs} - R_{NO3NH4})(1+R_{ON})}{(R_{ON} - R_{NO3NH4})(1+R_{obs})} \quad (3)$$

199 The nitrate functionality from organic nitrate was calculated as:

200 $$NO_{3,ON} = ON_{frac} \times NO_3^- \quad (4)$$

201 Thus, the nitrate functionality from inorganic nitrate (assuming NH_4NO_3 is the solely important
202 inorganic nitrate in the submicron mode) can be calculated as:

203 $$NO_{3,AN} = \left(1 - ON_{frac}\right) \times NO_3^- \quad (5)$$

204 The accurate estimation of the total mass of ON via this method is uncertain as the actual
205 molecular weight of the particle-phase species is unclear. The mass range of ON is estimated by
206 assuming that the average molecular weights of organic molecules with nitrate functional groups
207 are 200 to 300 g mol^{-1} (Surratt et al., 2008; Rollins et al., 2012). Previous work found that the
208 $NO_3^{\cdot}$ reaction with monoterpenes resulted in significant SOA formation and that a hydroperoxy

209 nitrate ($C_{10}H_{17}NO_5$) was likely a major $NO_3^{\cdot}$-oxidized terpene product in the southeastern U.S.
210 (Ayres et al., 2015). Here, we use the molecular weight of $C_{10}H_{17}NO_5$ (231 g mol^{-1}) to calculate
211 the ON mass. Example periods of significant ON contribution to PM are given in Fig. S4. While
212 the values of ON concentration estimated using this method are presented in the text, the result
213 of estimated ON including uncertainties is available in Table S2.

214 **2.3.2 PMF Analysis**

215 The PMF technique has been used widely for source apportionment (Paatero and Tapper,
216 1994), including with HR-TOF-AMS data (Ulbrich et al., 2009; Zhang et al., 2011). The
217 high-resolution NR-PM_1 OA mass spectra matrix (mass-to-charge ratio, m/z =12 to m/z=130)
218 and the associated error matrix obtained by using PIKA v 1.19 D were used for PMF analysis.
219 Data were prepared according to the protocol proposed by Ulbrich et al. (2009) and Zhang et al.
220 (2011) prior to PMF analysis. The PMF model was used to decompose the measured OA mass
221 spectra matrix by solving:

222 $$X = GF + E = \sum_{p=1}^{J} G_{ip} F_{pj} + E_{ij} \quad (6)$$

223 where X is the $m \times n$ matrix of measurement data, the *m* rows of X are the OA mass spectra
224 measured at each time step, the *n* columns of X are the time series of each organic m/z, and *p* is
225 the number of factors. G_{ip} is the matrix that denotes the contributions of factor *p* at time step *i*,
226 and F_{pj} represents the factor mass spectral profiles. E is the residual matrix. The least-squares
227 algorithm is used to fit the data to minimize iteratively a quality of fit parameter, Q:

228 $$Q = \sum_I \sum_J (E_{ij}/\sigma_{ij})^2 \quad (7)$$

229 where σ_{ij} is the matrix of estimated errors of the data.

Solutions using PMF with 2 to 7 factors were explored. The best solution with the optimum number of factors was evaluated carefully using an open source PMF evaluation tool (PET v 2.08D, (Ulbrich et al., 2009)) following the procedures described in Zhang et al. (2011). Selection criteria included 1.) variation of the ratio of Q to expected Q_{exp} ($mn-p(m+n)$, the degrees of freedom of the fitted data (Paatero et al., 2002)) after adding an additional factor, 2.) agreement between the reconstructed OA mass concentrations and the measured concentrations, 3.) scaled residuals for the different ion fragments included in the dataset and variations of the residual of the solution as a function of time, 4.) agreement between factor time series and time series of external tracers/individual ions, and 5.) examination of factor profiles. The last two are considered to determine the physical meaningfulness of the factors. The PMF solution with factor numbers greater than five and four for winter and summer dataset, respectively, yielded no new distinct and physical meaningful factors. The Q/Q_{exp} and the factors obtained for different FPEAK (from -1 to 1 with a step value of 0.2) values resulted in a small difference in the OA components. Because of the lowest Q/Q_{exp} and because the use of FPEAK values different from 0 did not improve the correlations between PMF factors and potentially associated tracers, the five- and four-factors solutions with FPEAK=0 can be well interpreted in winter and summer, respectively. The convergence of the PMF model containing five- and four-factors was examined by running each model from fifteen different starting values (SEEDs 0-30 with a step value of 2). The small variation observed in Q/Q_{exp} and the mass fraction of different factors as SEED changed indicates the solutions were stable. As a result, SEED 0 was chosen for the final solution. The factors were interpreted as hydrocarbon-like OA (HOA), biomass burning OA (BBOA), cooking OA (COA, identified only in the winter campaign), and two oxidized OA

(named less-oxygenated (LO-) OOA and more-oxygenated (MO-) OOA). The data treatment, factor selection and interpretation are detailed in the SI. As suggested by El-Sayed et al. (2016), drying of aerosol water may have led to the evaporation of condensed-phase organics. Thus, the resolved mass concentrations of OA factors here are a lower-bound, conservative estimate due to losses of aqueous-SOA in the dryer element.

2.3.3 Estimation of Aerosol Liquid Water Content (LWC)

Aerosol LWC includes water associated with inorganic aerosol and OA, which were calculated using a thermodynamic model and an empirical method, respectively. Inorganic LWC (W_i) in mol L^{-1} was predicted by ISORROPIA-II in forward mode (Fountoukis and Nenes, 2007). Inputs for ISORROPIA-II include inorganic aerosol mass concentrations (SO_4^{2-}, inorganic NO_3^-, and NH_4^+) and meteorological parameters (temperature and RH). Calculation empirical of organic LWC (W_O) follows (Petters and Kreidenweis, 2007; Guo et al., 2015):

$$W_O = \frac{m_{org}\rho_w}{\rho_{org}} \frac{\kappa_{org}}{(1/RH - 1)} \quad (8)$$

where m_{org} is the organic mass concentration (μg m^{-3}) and ρ_w is the density of water (1 g cm^{-3}). The organic density (ρ_{org}, g cm^{-3}) was estimated using an empirical equation based on elemental ratios (Kuwata et al., 2012; Guo et al., 2015):

$$\rho_{org} = 1000 \times \left[\frac{12 + \frac{H}{C} + 16 \times \frac{O}{C}}{7.0 + 5 \times \frac{H}{C} + 4.15 \times \frac{O}{C}}\right] \quad (9)$$

The hygroscopicity of SOA generated during chamber studies under sub-saturated regimes depends on the OA degree of oxidation (Prenni et al., 2007; Jimenez et al., 2009; Petters et al., 2009; Chang et al., 2010). A simple linear relationship between the OA degree of oxidation

(defined as the fraction of the total signal at *m/z* 44, f_{44}) and hygroscopicity (κ_{org}) is used (Duplissy et al., 2011):

$$\kappa_{org} = 2.2 \times f_{44} - 0.13 \quad (10)$$

The total LWC is then found by summing the water content associated with each mass fraction:

$$LWC = W_i + W_O \quad (11)$$

3 Results and Discussion

3.1 Temporal Dependences of Submicron Aerosol Composition

Campaign overview data for winter and summer are shown in Table 1 and Fig. 1. This includes meteorological parameters (e.g., temperature, RH, radiometer, precipitation, wind direction and speed), trace gases (e.g., CO, SO_2, NO_2, and O_3), and chemically resolved NR-PM_1 concentrations.

Data indicate that the average concentration of NR-PM_1 during winter campaign was 6.0 ± 3.7 μg m^{-3}, ranging from 0.5 to 14.8 μg m^{-3}. Mass loadings of NR-PM_1 at this measurement site are relatively smaller than at a site near the HSC in winter 2015 (10.8 μg m^{-3} (Wallace et al., 2018)), perhaps suggesting a weaker industrial influence at the UHSL site.

The average concentration of NR-PM_1 during summer was 3.6 ± 1.7 μg m^{-3}, ranging from 0.3 to 13.7 μg m^{-3}. For comparison, a summer campaign in 2006 on an elevated building near downtown Houston showed an average NR-PM_1 concentration of approximately 11 μg m^{-3} (Cleveland et al., 2012). An elevated NR-PM_1 episode was observed from May 28-31 (Fig. 1(J)), with high solar radiation and O_x (O_x = NO_2 + O_3) levels during the daytime, and high RH at

night, resulting in OA becoming the largest fractional species, likely due to gas-phase photochemical production of SOA together with the nighttime increase of SOA associated with high RH, lowered boundary layer and cooler temperatures.

In winter, OA was the largest component of NR-PM_1, accounting for 38 ± 13% on average of the total mass, followed by SO_4^{2-} (23 ± 11%), NO_3^- (23 ± 11%), NH_4^+ (15 ± 5%) and Cl^- (1 ± 0.2%) (Fig. 2). Primary OA (POA=HOA+BBOA+COA) was responsible for 61 ± 19% of OA mass. Secondary species (SO_4^{2-}+NO_3^-+NH_4^++LO-OOA+MO-OOA) accounted for ~76 ± 21% of NR-PM_1 mass, which is higher than that in winter in Seoul (Kim et al., 2017) and Beijing (Hu et al., 2016).

In contrast to winter, OA during the summer campaign constituted on average 47 ± 18% of NR-PM_1 mass, and SO_4^{2-} was the second largest component (36 ± 15%), followed by NH_4^+ (14 ± 5%). NO_3^- only accounted for 2 ± 1% of NR-PM_1 mass in the summer, and Cl^- contributed 1 ± 0.5% of NR-PM_1 mass. The increased planetary boundary layer (PBL) height in summer (Haman et al., 2012) likely contributed to relatively lower trace gas and NR-PM_1 levels in the summer. Secondary species contributed ~88 ± 15% of NR-PM_1 mass, indicating that the relative importance of secondary aerosol formation increased during summer as compared to winter, especially for species such as SO_4^{2-} and MO-OOA.

The total OA displayed high values during the nighttime hours in both winter and summer, maintaining a high level until morning rush hour, and then decreasing to a minimum value after 9:00 (Fig. 3). The summertime OA presented a small peak at noon, suggesting that photochemical formation of OA played a more important role in summer than in winter. Increasing ambient temperature and PBL height after sunrise causes re-partitioning to the gas

315 phase, likely contributing to the decrease of OA, LO-OOA and ON during daytime.

316 Contributions of PMF factors to wintertime and summertime OA show significant
317 differences. For wintertime OA, on average, BBOA contributed to 26% of OA mass; MO-OOA
318 and COA made the same contributions of 22% to total OA mass. The LO-OOA accounted for 17%
319 of OA mass, followed by HOA (13%). The POA constituted more than half of OA mass (61%),
320 with the remainder of being OOA (39%). In the summer, LO-OOA represented the largest
321 fraction of the OA mass (54% on average), followed by MO-OOA (23%), HOA (15%) and
322 BBOA (8%). In the case of summer, OOA constituted 77% of OA and 36% of total NR-PM_1
323 mass, which are almost two times their relative contributions in winter. The time series of mass
324 concentrations of NR-PM_1 species (Fig. 1) and OA factors (Fig. 4) in summer were relatively
325 stable and repeatable, while they varied dramatically in winter due to the different
326 meteorological conditions.

327

328 **3.2 Seasonal Variation of the Formation of Sulfate and Nitrate**

329 During the summer campaign, the prevailing southerly winds from the Gulf of Mexico carry
330 marine aerosols to Houston (Schulze et al., 2018), resulting in a relatively high fraction of SO_4^{2-}.
331 As shown in Fig. 1(G, J), the increased contribution of SO_4^{2-} occurred when winds originated
332 from the south at a high speed (e.g., May 16-27), while the contribution of SO_4^{2-} decreased
333 significantly when winds originated from the north (e.g., May 10th and May 13-15). During
334 periods of southerly winds, O/C and OM/OC were relatively higher (Fig. S2(C)). In addition,
335 elevated SO_2 plumes were recorded during periods of southerly winds (Fig. 1(G, H)), potentially
336 as a result of emissions from the Parish coal-fired power plant. In contrast to SO_4^{2-}, the fractional

337 contribution of NO_3^- and OA increased greatly when the winds were not southerly. Primary
338 pollutants such as CO and NO_2, were elevated when winds were northerly (Fig. 1(H)),
339 accompanied by lower O/C and higher H/C ratios during the corresponding periods (Fig. S2(C),
340 e.g., May 1st, 2rd, 10th, 15th).

341 Diurnal patterns of NR-PM_1 and other species in the winter and summer (Fig. 3) suggest
342 significant seasonal dependence of sources and formation processes of NR-PM_1 species in
343 Houston. In the case of SO_4^{2-}, the diurnal pattern displayed a daytime peak in both winter and
344 summer, with the peak much more pronounced in summer mid-day. In winter, the f_{SO4} (mole
345 ratio of $[SO_4^{2-}]$ to the sum of $[SO_2]$ and $[SO_4^{2-}]$) and LWC have concurrent peak values during
346 the night (Figure 5). However, there is no obvious correlation between f_{SO4} and LWC in summer,
347 though a moderate correlation (r = 0.44) was found in winter. By comparing the diurnal plots of
348 sulfate in winter and summer, it appears that sulfate generated from aqueous chemistry
349 accounted for more mass and a greater fraction of total sulfate production in winter than in
350 summer.

351 The total nitrate concentration was higher in winter than in summer. The $NO_3^-{}_{,AN}$ was very
352 low in summer due to its thermal instability under high temperature, while it was relatively
353 enhanced in winter. According to the NO_x^+ ratio method described in Sec. 2.3.1, the mass
354 fraction of $NO_3^-{}_{,AN}$ in total nitrate was in the range of 65-66% in winter, and in the range of
355 19-39% in summer. The averaged bound concentrations of $NO_{3,ON}$ ranged from 0.22-0.34 μg m^{-3}
356 in winter, and 0.05-0.06 μg m^{-3} in summer. The seasonal variation of $NO_3^-{}_{,AN}$ is much stronger
357 than that of $NO_{3,ON}$. This is in accordance with previous observations in Atlanta, Georgia and
358 Centreville, Alabama (Xu et al., 2015).

359 The diurnal profiles of $NO_{3,ON}$ show that it reached peak value before dawn in both seasons
360 (Fig. 5). However, $NO_3^-{}_{,AN}$ presents a bimodal diurnal profile in both seasons. The $NO_3^-{}_{,AN}$,
361 which increased from late afternoon and peaked at 2:00-4:00, was likely formed through
362 nighttime chemistry from dinitrogen pentoxide (N_2O_5) hydrolysis, as the LWC displayed a trend
363 similar to that of $NO_3^-{}_{,AN}$, This was corroborated by the observation of O_x (>25 ppb), which is
364 needed to form N_2O_5 (via $NO_3^{\cdot}$). The second peak observed during morning rush hour was likely
365 formed though photochemical processing of NO_x emitted from vehicles because the traffic flow
366 and O_x level are elevated during morning rush hour. The decreasing trend of $NO_3^-{}_{,AN}$ after 9:00 is
367 presumed to be a result of enhanced PBL height and evaporation.
368 The estimated ON accounted for 4-8% of the total NR-PM_1 and 9-17% percent of the OA in
369 summer and 12-27% of the total NR-PM_1 and 31-66% percent of the OA in winter, comparable
370 to other studies (Fry et al., 2009; Rollins et al., 2010; Xu et al., 2015; Berkemeier et al., 2016). A
371 proxy for $NO_3^{\cdot}$ production rate is based on the product of the observations of [NO_2] and [O_3]
372 (Rollins et al., 2012), where brackets represent mixing ratios in ppb. The O_x (> 25 ppb) and
373 elevated NO_x observed at night in summer (Fig. 3) resulted in rapid $NO_3^{\cdot}$ formation. Thus, the
374 concurrent enhancement in ON and O_3 times NO_2 occurring during nighttime (Fig. S4) likely
375 indicates the nocturnal $NO_3^{\cdot}$-initiated oxidation of anthropogenic and biogenic VOCs, with the
376 latter probably larger than the former (Brown et al., 2013). The high N/C ratio of LO-OOA,
377 concurrent peak value in LO-OOA and ON (MW=231 g mol^{-1}) during nighttime hours (Fig. 3),
378 and appreciable correlation of LO-OOA and ON in summer (r = 0.73) (Fig. 4) together suggest
379 that particle-phase ON from $NO_3^{\cdot}$-initiated chemistry contributed to nighttime LO-OOA in
380 summer.

3.3 Effects of Aqueous-phase and Photochemical Oxidation on OOA Formation

On average, OOA accounted for 39 ± 19% of OA mass in winter but increased to 77 ± 16% in summer. Note that MO-OOA accounted for more than half of OOA in winter (56%), indicating the more important role of MO-OOA in winter as compared to LO-OOA on a relative basis. In contrast, LO-OOA dominated OOA in summer (70%). The mass spectra of MO-OOA in winter and summer are similar (Fig. 6, r = 0.84) as are the extent of oxidation (O/C = 1.10 versus 1.07). However, LO-OOA in winter showed a different spectral pattern compared with that in summer. The mass spectrum of LO-OOA in winter was characterized by high *m/z* 32 (mainly CH_4O^+) and 46 (mainly $CH_2O_2^+$) peaks, resulting in a relatively high O/C (0.89) in winter that suggest LO-OOA in winter was more aged than that in summer (O/C=0.74).

Sun et al. (2016) reported a unique OOA in ambient air, termed aq-OOA (aqueous-phase-processed SOA), that strongly correlated with particle LWC, sulfate and S-containing ions. As shown in Table 2, by comparing the mass spectra of OOA in this work with aq-OOA, it is found that the mass spectra of MO-OOA in winter in this study presents a much stronger correlation (r =0.96) with aq-OOA, than does LO-OOA in winter in this study (r =0.75). Both MO-OOA and LO-OOA in summer highly correlated with aq-OOA. This result indicates that the formation of LO-OOA in summer and MO-OOA in both seasons may involve aqueous-phase chemistry.

Assuming that OOA deduced from PMF analysis can be used as a surrogate of SOA (Wood et al., 2010; Xu et al., 2017), the two OOA were used to investigate the formation mechanisms and evolutionary processes of SOA. Previous studies have found SOA correlated well with odd

403 oxygen (O_x) in many cities (Wood et al., 2010; Sun et al., 2011; Hayes et al., 2013; Zhang et al.,
404 2015; Xu et al., 2017) and that SOA formation is significantly impacted by aqueous-phase
405 processing (Lim et al., 2010; Ervens et al., 2011; Xu et al., 2017). The relationships between
406 OOA factors and O_x/LWC were used as the metrics to characterize SOA formation mechanisms
407 associated with photochemistry/aqueous oxidation chemistry (Xu et al., 2017).

408 Fig. 7 (A, B) indicates the LWC frequency distribution. Winter LWC are binned in 5 μg m^{-3}
409 increments from 0 to 20 μg m^{-3}. Data in the ranges of 20 to 30 μg m^{-3}, 30 to 50 μg m^{-3}, 50 to 80
410 μg m^{-3}, and 80 to 120 μg m^{-3} are shown as 25, 40, 65 and 100 μg m^{-3}, respectively. Summer
411 LWC are binned in 2.5 μg m^{-3} increments from 0 to 15 μg m^{-3}. The bins shown as 17.5 and 27.5
412 μg m^{-3} represent data from 15 to 20 μg m^{-3} and 20 to 35 μg m^{-3}. It should be noted that a fit for
413 the binned data likely results in an increase in R^2 compared to the fit for the original data. For
414 example, the correlation coefficient of the fit for the averaged binned wintertime MO-OOA
415 (increased from 0.57 to 0.98 μg m^{-3}) versus LWC (increased from 2.5 to 40 μg m^{-3}) is 0.55,
416 while it is 0.06 for the original data (Figure 7(I)).

417 The data associated with the artificially created bins in both seasons did not pass the normal
418 test and homogeneity test of variances. The statistical significance of differences between bins
419 was then tested using the Kruskal-Wallis analysis of variance (K-W ANOVA). The differences
420 between winter and summer data of the bins were significant. Thus, the Dunn-Bonferroni test
421 was performed for the *post-hoc* pairwise comparisons. It was found that the difference of all
422 measured variables in different bins shown in Fig. 7 were significant (p<0.01). The results can be
423 found in Tables S6-S7. Fig. 7(C, D) presents a clear positive trend of RH as a function of LWC
424 in both winter and summer which implies an increased potential for aqueous-phase processing at

high RH level, enhanced by low wind speed that allows accumulation of pollutants (Fig. 7(E, F)). The patterns of other parameters as LWC increases in winter were different from those in summer.

The variation of binned mean OA mass against LWC presents significant seasonal difference (Fig. 7(A, B)). In winter, the OA mass increased when LWC increased from 2.5 to 12.5 μg m^{-3} but decreased as the LWC increased further. In summer, the OA mass slightly decreased when LWC increased from 1.25 to 6.25 μg m^{-3} but slightly increased when LWC increased further, suggesting the production of OA is not as strong as that in winter because of the relatively lower LWC in summer.

The winter LO-OOA mass decreased dramatically when LWC>12.5 μg m^{-3} (RH>80%, Fig. 7(C)) while MO-OOA continues increasing until LWC> 40 μg m^{-3}. This result indicates that wet removal may dominate under an extremely high RH environment coupled with stagnant air (WS <2 m/s Fig. 7(E)) or that LO-OOA production decreased at extremely high LWC level (Fig. 7(A)). Specifically, average LO-OOA (Fig. 7(G, H)) in winter increased from 0.3 to 0.9 μg m^{-3} when LWC increased from 2.5 to 7.5 μg m^{-3} but decreased as the LWC increased further, particularly when LWC >40 μg m^{-3}. The slope of this decrease was approximately -0.008 μg LO-OOA μg^{-1} LWC. Fig. 7(A) shows that 64% of the data points were observed in the situation of low LWC (<12.5 μg m^{-3}, RH<80%), when the increase of LO-OOA was largest.

In contrast, LO-OOA in summer showed a decreasing trend under low LWC level (LWC<6.25 μg m^{-3}, RH<80%) but an increasing trend from approximately 0.77 μm^{-3} to 1.8 μg m^{-3} as LWC increased from 6.25 to 27.5 μg m^{-3}, a slope of 0.053 μg LO-OOA μg^{-1} LWC. The relatively high summer LO-OOA under low LWC level was likely more regional, with

447 contributions from possibly transported non-aqueous OOA, as the wind speed in this case was
448 relatively high and RH was low. The production of LO-OOA under high LWC level may have
449 been enhanced by local aqueous-phase heterogeneous chemistry.

450 MO-OOA slightly increased during both seasons as LWC increased (Fig. 7(I, J)). In winter,
451 MO-OOA presented an increasing trend from 0.57 to 0.98 μg m^{-3} when LWC increased from 2.5
452 to 40 μg m^{-3} but decreased slightly as the LWC increased further. The slope of this increase was
453 approximately 0.008 μg MO-OOA μg^{-1} LWC with correlation coefficient of 0.55. In summer,
454 MO-OOA appears to increase from 0.49 to 0.64 μg m^{-3} when LWC increased from 2.5 to 27.5 μg
455 m^{-3}, with slope of 0.005 μg MO-OOA μg^{-1} LWC (R^2=0.34). In winter, because of the decrease in
456 LO-OOA with LWC, the relative fraction of MO-OOA increases as LWC increases.

457 The mutual effect of aqueous-phase and photochemistry on OOA formation prevents solely
458 evaluating the role of the two processes. Sullivan et al. (2016) reported multiple lines of evidence
459 for local aq-SOA formation observed in the Po Valley, Italy during times of increasing RH,
460 which coincided with dark conditions. Thus, the daytime data were separated to examine the
461 variation of OOA against O_x. The relationship between OOA and aqueous-phase chemistry was
462 investigated further by excluding the daytime data, with the aim of diminishing the instantaneous
463 influence of photochemistry on the data. To do so, nighttime and daytime were based on sunrise
464 and sunset in Houston during the two campaigns
465 (https://www.timeanddate.com/sun/usa/houston). On average, the day lengths are 11 h 10 min
466 and 13 h 35 min for the campaigns in February and May, 2014, respectively.

467 A potential linear relationship between OOA and LWC for the nighttime data was
468 investigated by fitting the data with a locally weighted scatter plot smoothing algorithm

(LOWESS, (Cleveland, 1981)). According to the LOWESS curves for the original nighttime data and the resampled data obtained by a bootstrap method (Figs. S14-15), there likely exists a linear relationship between LO-OOA and LWC for data points with LWC less than 20 μg m^{-3} and greater than 6 μg m^{-3} for the winter and summer periods, respectively. As for MO-OOA, such a linear relationship likely exists when LWC is less than 50 and 7 μg m^{-3} for the winter and summer periods, respectively.

Figure 8 presents the scatter plots of OOA versus LWC during nighttime for the two campaigns. The green dots denote the increasing trend of OOA against LWC. It is found that the increase of wintertime LO-OOA under low LWC level (<20 μg m^{-3}) during the night is stronger than that shown in Fig. 7 (G). The nighttime LO-OOA linearly increased from 0.04 to 0.64 μg m^{-3} when LWC increased from 2.5 to 17.5 μg m^{-3}, a slope of 0.033 μg LO-OOA μg^{-1} LWC. This result indicates that the nighttime production of LO-OOA in winter may be more likely formed via aqueous-phase chemistry in aerosol liquid water than that in day time. The production of LO-OOA under high LWC level (LWC>6.25 μg m^{-3}) in summer during nighttime (0.055 μg LO-OOA μg^{-1} LWC) was comparable to the increase rate of whole dataset (0.053 μg LO-OOA μg^{-1} LWC). The nighttime increasing trends of MO-OOA against LWC in both seasons are stronger than those shown in Fig. 7(I, J) with respect to the correlation coefficient values. The slope of nighttime increase of MO-OOA against LWC during the winter campaign was 0.013 μg MO-OOA μg^{-1} LWC, which is 1.7 times the slope for the whole dataset (daytime and nighttime). For the summer campaign, the increase of nighttime MO-OOA is 2.2 times the rate for the whole dataset.

These results suggest that aqueous-phase processing likely has a strong positive impact,

491 particularly at night, on the production of MO-OOA in the two seasons except for instances
492 when LWC exceeds 100 μg m^{-3} in winter. It also appears to facilitate the local production of
493 LO-OOA under low LWC level (<17.5 μg m^{-3}) in winter and under relatively high LWC level
494 (>6.25 μg m^{-3}) in summer.

495 As mentioned previously, ON contributes significantly to summertime LO-OOA, and the
496 concurrent enhancement in ON and LO-OOA during night was associated with elevated RH (Fig.
497 3). A previous study found that the partitioning of organic compounds to the particle phase was
498 significantly increased at elevated RH levels (70%) in an urban area dominated by biogenic
499 emissions in Atlanta (Hennigan et al., 2008). The correlation of ON and LO-OOA in summer
500 nighttime (r=0.76) was stronger than that during daytime (r =0.53). This is likely due to the
501 higher ON yields from NO_3˙-initiated chemistry involving BVOCs during nighttime compared to
502 hydroxyl-radical-initiated chemistry involving BVOCs during daytime. Additionally, the
503 concurrent enhancement of the LWC and nitrate functionality from organic nitrate during
504 nighttime demonstrates that the LWC does not inhibit increases in concentration, as might be
505 expected if hydrolysis occurred rapidly.

506 Fig. 9(A, B) presents the frequency distribution of O_x. Winter O_x are binned in 10 ppb
507 increments from 0 to 60 ppb. The range for summer is 20 to 70 ppb. The data associated with the
508 artificially created O_x bins in both seasons did not pass the normal test and homogeneity test of
509 variances. The K-W ANOVA for winter and summer data of the bins were significant. The
510 Dunn-Bonferroni test for the *post-hoc* pairwise comparisons shows that the difference of
511 measured variables among different bins shown in Fig. 9 were significant (Tables S8-S9). The
512 clear positive relationship between solar radiation and O_x is shown in Fig. 9 (C, D), and the

513 negative relationship between RH and O_x is shown in Fig. 9 (E, F), confirming strong
514 atmospheric photochemical activity associated with high O_x periods.

515 The variations of LO-OOA and MO-OOA showed substantially different patterns with
516 increases of O_x in winter and summer. In winter, LO-OOA and MO-OOA showed comparable
517 increasing trends at low O_x level (<35 ppb), with MO-OOA having a stronger response. The
518 LO-OOA increased from 0.13 to 0.72 μg m^{-3} when O_x increased from 5 to 35 ppb but decreased
519 as the O_x increased further. The slope of this increase was approximately 0.023 μg LO-OOA
520 ppb^{-1} O_x. MO-OOA increased from 0.13 to 0.88 μg m^{-3} when the O_x increased from 5 to 35 ppb,
521 with a slope of 0.027 μg MO-OOA ppb^{-1} O_x. This leads to a maximum in the mass fraction of
522 MO-OOA as O_x approached its highest observed levels.

523 In summer, there is a clear decreasing trend of RH with increases of O_x. As discussed
524 previously, the high level of summertime LO-OOA likely was associated with high LWC.
525 Therefore, the high mass fraction of LO-OOA at the lowest O_x level (<20 ppb) associated with
526 the high RH/LWC was likely from aqueous-phase chemistry. After excluding low-O_x data (<20
527 ppb), LO-OOA showed a much stronger response to O_x than did MO-OOA. The summer
528 LO-OOA increased from approximately 0.6 to 1.8 μg m^{-3} when O_x increased from 25 to 65 ppb,
529 a slope of 0.03 μg LO-OOA ppb^{-1} O_x. This increase was likely in the case of low RH conditions
530 (<80%, Fig. 7 (D)), when aqueous-phase chemistry was less likely to promote the production of
531 LO-OOA (Fig. 7 (H)). Summer MO-OOA increased from 0.36 to 0.67 μg m^{-3} when O_x increased
532 from 25 to 55 ppb but decreased as the O_x increased further. The slope of this increase was 0.007
533 μg MO-OOA ppb^{-1} O_x. Contrary to winter, LO-OOA in summer responded more strongly to
534 increases of O_x than MO-OOA did.

The relationship of OOA versus O_x was examined further by excluding nighttime data. According to the LOWESS curves for the original daytime data and the resampled data obtained using a bootstrap method (Figs. S16-17), there likely exists a linear relationship between LO-OOA and O_x when O_x is less than 35 ppb and greater than 20 ppb for the winter and summer period, respectively. As for MO-OOA, the linear relationship likely exists for data points with O_x less than 35 ppb for the winter period, but it is less prominent.

Figure 10 presents the scatter plots of daytime OOA versus O_x for the winter and summer campaign. The daytime responses of LO-OOA and MO-OOA to O_x in winter were ~1.5 times that for the whole dataset (Fig. 9 (G, I)), and the increase rate of MO-OOA was higher than that of LO-OOA. In summer, the slope of the daytime increase of LO-OOA was 1.24 times that for the whole campaign (Fig. 9 (H)). These results suggest that the photochemical enhancement of OOA in winter on a per-O_x basis was more prominent than that in summer. For the summer campaign, the formation of LO-OOA appears to be more strongly linked to photochemistry compared to MO-OOA.

The combined effects of photochemistry and aqueous-phase chemistry on OOA composition during winter and summer are further demonstrated in Fig. 11. The ratio of MO-OOA/LO-OOA in winter showed the highest values on the left-top corner in Fig. 11 (A), suggesting photochemical processing was likely responsible for MO-OOA formation, under low LWC levels (< 10 μg m^{-3}). Additionally, data with high MO-OOA/LO-OOA on the right-bottom corner in Fig. 11 (A) indicate the important role of aqueous-phase chemistry under low O_x and high LWC levels. Overall, the concentration of MO-OOA in winter increased as O_x/LWC increased, whereas LO-OOA markedly decreased. This result indicates both photochemical and

aqueous-phase processing played a more important role in enhancing MO-OOA than LO-OOA in winter.

In summer, data points with low MO-OOA/LO-OOA value on the left-top of Figure 11 (B) illustrated that LO-OOA was enhanced in high-O_x and low-LWC conditions, though the low MO-OOA/LO-OOA values are not confined to just the top left. In case of high LWC level (LWC> 6.5 μg m^{-3}), MO-OOA/LO-OOA were much lower (on the right of Figure 11 (B), particularly when LWC> 10 μg m^{-3}). Although MO-OOA increased with LWC and O_x, the increase of LO-OOA was more significant. The effects of both photochemistry (≥ 25 ppb) and aqueous-phase chemistry (≥ 6.5 μg m^{-3}) were more relevant for the formation of LO-OOA than MO-OOA. On average, the mass concentration of LO-OOA was elevated by nearly 1.2 μg m^{-3} as a ~20 μg change in LWC (increased from 6.25 μg m^{-3} to 27.5 μg m^{-3}, Fig. 7 (H)), which is equivalent to a 40 ppb change in O_x (increased from 25 ppb to 65 ppb, Fig. 9 (H)). This result further suggests that the aqueous-phase chemistry is comparable to photochemistry in processing LO-OOA in summer.

4 Conclusions

Seasonal characterization of NR-PM_1 collected using HR-ToF-AMS near Houston in 2014 demonstrated that the mass loading, diurnal patterns, and important formation pathways of NR-PM_1 vary seasonally. The OA was the largest component of NR-PM_1 mass, on average, accounting for 38% and 47% of the mass loadings in winter and summer, respectively, which is less than that in the north part of Houston, which is influenced by high biogenic emission rates. Nitrate was the second largest component in winter (23%) but accounted for only 2% of NR-PM_1

579 mass in summer; SO_4^{2-} was the second largest component in winter (23%) and summer (36%),
580 respectively. ON, on average accounted for 31-66 and 9-17 % of OA during winter and summer
581 campaign, respectively. The summertime ON correlated very well with LO-OOA and
582 concurrently peaked at nighttime. It is likely that ON from NO_3 · -initiated oxidation of BVOC
583 in the forested northeastern Houston contributed greatly to nighttime LO-OOA in summer and
584 that LWC did not inhibit resulting concentration growth.

585 Contributions of factors to wintertime and summertime OA show distinct differences. For
586 wintertime OA, on average, BBOA contributed 26% of OA mass, and MO-OOA and COA made
587 the same contribution of 22% to total OA mass. LO-OOA accounted for 17% of OA mass,
588 followed by HOA (13%). In the summer, LO-OOA represented the largest fraction of the OA
589 mass, 54% on average. The second largest contributor was MO-OOA (23%). Together, POA
590 constituted more than half of OA mass (61%) in winter, while it accounted for 23% of OA mass
591 in summer, highlighting the enhanced impact of primary emissions on OA level during
592 wintertime. Secondary aerosols account for ~76% and 88% of NR-PM_1 mass in winter and
593 summer, respectively, indicating NR-PM_1 mass was likely driven mostly by secondary aerosol
594 formation.

595 The two proxies of SOA (LO-OOA and MO-OOA) presented seasonal differences in their
596 spectral patterns, oxidation degrees and contributions to SOA. MO-OOA showed a higher
597 contribution to SOA than LO-OOA in winter (56% vs. 44%). In contrast, LO-OOA dominated
598 SOA in summer (70%). Our results indicate that both photochemical and aqueous-phase
599 chemistry, as suggested by relationships to O_x and LWC, played important roles in the formation
600 of MO-OOA and LO-OOA. Aqueous-phase processing likely has strong positive impact on the

formation of MO-OOA in the two seasons, especially in winter. The relationships between MO-OOA and LWC were 0.008 and 0.005 μg MO-OOA μg^{-1} LWC during winter and summer, respectively. Wet removal or decreased formation rates likely limit MO-OOA when LWC exceeds 100 μg m^{-3} in winter. The relative importance of aqueous-phase chemistry versus photochemistry in processing LO-OOA was dependent on RH. Aqueous-phase processing potentially facilitated the local formation of wintertime LO-OOA at low LWC level (<17.5 μg m^{-3}, RH<80%), with a stronger dependence (0.033 μg LO-OOA μg^{-1} LWC) than MO-OOA. In summer, the formation of LO-OOA may have been enhanced by aqueous-phase processing at relatively high LWC level (>6.25 μg m^{-3}, RH>80%) with a slope of 0.053 μg LO-OOA μg^{-1} LWC, while LO-OOA was likely transported non-aqueous regional OOA when LWC < 6.25 μg m^{-3}. These increases of OOA in relation to LWC were greatly enhanced during nighttime. Aqueous-phase chemistry also appears important in the formation of summertime LO-OOA at low atmospheric oxidative capacity (O_x < 20 ppb). In general, summertime LO-OOA showed a much stronger response to O_x than did MO-OOA, with a slope of 0.030 μg LO-OOA ppb^{-1} O_x. LO-OOA in summer was elevated by nearly 1.2 μg m^{-3} as a ~20 μg change in LWC, which is equivalent to a 40 ppb change in O_x.

Acknowledgments

The authors would like to acknowledge Yele Sun (Institute of Atmospheric Physics, Chinese Academy of Sciences) for providing the aq-OOA mass spectra, and Qiao Zhu (Peking University Shenzhen Graduate School) for assistance in the calculation of organic nitrates and PMF analysis. The scholarships provided by China Scholarship Council to Qili Dai and Xiaohui Bi are

gratefully acknowledged. Support of the Houston Endowment in development and deployment of the MAQL also is gratefully acknowledged. Datasets are available by contacting the corresponding author.

Author contribution. Qili Dai performed the data analysis and wrote the manuscript. Robert J. Griffin and Yinchang Feng assisted heavily with manuscript development and editing. Henry W. Wallace, Alexander A.T. Bui, James H. Flynn, and Barry L. Lefer contributed to data collection during the field campaigns. Benjamin C. Schulze, Henry W. Wallace, Alexander A.T. Bui and Nancy P. Sanchez contributed with data analysis. Xiaohui Bi, Benjamin C. Schulze, Alexander A.T. Bui, Fangzhou Guo, Nancy P. Sanchez, and James H. Flynn provided helpful comments and edits.

Competing interests. The authors declare that they have no conflict of interest.

References

Allen, D. T., and Fraser, M.: An overview of the Gulf Coast Aerosol Research and Characterization Study: The Houston Fine Particulate Matter Supersite, J. Air Waste Manage., 56, 456-466, http://doi.org/10.1080/10473289.2006.10464514, 2006.

Atkinson, D. B., Massoli, P., O'Neill, N. T., Quinn, P. K., Brooks, S. D., and Lefer, B.: Comparison of in situ and columnar aerosol spectral measurements during TexAQS-GoMACCS 2006: testing parameterizations for estimating aerosol fine mode properties, Atmos. Chem. Phys., 10, 51-61, http://doi.org/10.5194/acp-10-51-2010, 2010.

Ayres, B. R., Allen, H. M., Draper, D. C., Brown, S. S., Wild, R. J., Jimenez, J. L., Day, D. A., Campuzano-Jost, P., Hu, W., de Gouw, J., Koss, A., Cohen, R. C., Duffey, K. C., Romer, P.,

647 Baumann, K., Edgerton, E., Takahama, S., Thornton, J. A., Lee, B. H., Lopez-Hilfiker, F. D.,
648 Mohr, C., Wennberg, P. O., Nguyen, T. B., Teng, A., Goldstein, A. H., Olson, K., and Fry, J.
649 L.: Organic nitrate aerosol formation via NO_3 + biogenic volatile organic compounds in the
650 southeastern United States, Atmos. Chem. Phys., 15, 13377-13392,
651 http://doi.org/10.5194/acp-15-13377-2015, 2015.
652 Bahreini, R., Ervens, B., Middlebrook, A. M., Warneke, C., de Gouw, J. A., DeCarlo, P. F.,
653 Jimenez, J. L., Brock, C. A., Neuman, J. A., Ryerson, T. B., Stark, H., Atlas, E., Brioude, J.,
654 Fried, A., Holloway, J. S., Peischl, J., Richter, D., Walega, J., Weibring, P., Wollny, A. G.,
655 and Fehsenfeld, F. C.: Organic aerosol formation in urban and industrial plumes near
656 Houston and Dallas, Texas, J. Geophys. Res., 114, D00f16,
657 http://doi.org/10.1029/2008jd011493, 2009.
658 Bates, T. S., Quinn, P. K., Coffman, D., Schulz, K., Covert, D. S., Johnson, J. E., Williams, E. J.,
659 Lerner, B. M., Angevine, W. M., Tucker, S. C., Brewer, W. A., and Stohl, A.: Boundary layer
660 aerosol chemistry during TexAQS/GoMACCS 2006: Insights into aerosol sources and
661 transformation processes, J. Geophys. Res., 113, D00f01,
662 http://doi.org/10.1029/2008jd010023, 2008.
663 Bean, J. K., Faxon, C. B., Leong, Y. J., Wallace, H. W., Cevik, B. K., Ortiz, S., Canagaratna, M.
664 R., Usenko, S., Sheesley, R. J., Griffin, R. J., and Hildebrandt, L: Composition and sources
665 of particulate matter measured near Houston, TX; Anthropogenic-biogenic interactions,
666 Atmos., 7, 73, https://doi.org/10.3390/atmos7050073, 2016
667 Berkemeier, T., Ammann, M., Mentel, T. F., Poschl, U., and Shiraiwa, M.: Organic Nitrate
668 Contribution to New Particle Formation and Growth in Secondary Organic Aerosols from
669 alpha-Pinene Ozonolysis, Environ. Sci. Technol., 50, 6334-6342,
670 http://doi.org/10.1021/acs.est.6b00961, 2016.
671 Boyd, C. M., Sanchez, J., Xu, L., Eugene, A. J., Nah, T., Tuet, W. Y., Guzman, M. I., and Ng, N.
672 L.: Secondary Organic Aerosol (SOA) formation from the β-pinene CNO3 system: effect of
673 humidity and peroxy radical fate, Atmos. Chem. Phys., 15, 7497–7522,
674 doi:10.5194/acp-15-7497-2015, 2015.
675 Brown, S. S., Dube, W. P., Bahreini, R., Middlebrook, A. M., Brock, C. A., Warneke, C., de
676 Gouw, J. A., Washenfelder, R. A., Atlas, E., Peischl, J., Ryerson, T. B., Holloway, J. S.,
677 Schwarz, J. P., Spackman, R., Trainer, M., Parrish, D. D., Fehshenfeld, F. C., and
678 Ravishankara, A. R.: Biogenic VOC oxidation and organic aerosol formation in an urban
679 nocturnal boundary layer: aircraft vertical profiles in Houston, TX, Atmos. Chem. Phys., 13,

11317-11337, http://doi.org/10.5194/acp-13-11317-2013, 2013.

Bruns, E. A., Perraud, V., Zelenyuk, A., Ezell, M. J., Johnson, S. N., Yu, Y., Imre, D., Finlayson-Pitts, B. J., and Alexander, M. L.: Comparison of FTIR and Particle Mass Spectrometry for the Measurement of Particulate Organic Nitrates, Environ. Sci. Technol., 44, 1056–1061, 2010.

Canagaratna, M. R., Jayne, J. T., Jimenez, J. L., Allan, J. D., Alfarra, M. R., Zhang, Q., Onasch, T. B., Drewnick, F., Coe, H., Middlebrook, A., Delia, A., Williams, L. R., Trimborn, A. M., Northway, M. J., DeCarlo, P. F., Kolb, C. E., Davidovits, P., and Worsnop, D. R.: Chemical and microphysical characterization of ambient aerosols with the aerodyne aerosol mass spectrometer, Mass Spectrom. Rev., 26, 185-222, http://doi.org/10.1002/mas.20115, 2007.

Canagaratna, M. R., Jimenez, J. L., Kroll, J. H., Chen, Q., Kessler, S. H., Massoli, P., Hildebrandt Ruiz, L., Fortner, E., Williams, L. R., Wilson, K. R., Surratt, J. D., Donahue, N. M., Jayne, J. T., and Worsnop, D. R.: Elemental ratio measurements of organic compounds using aerosol mass spectrometry: characterization, improved calibration, and implications, Atmos. Chem. Phys., 15, 253-272, http://doi.org/10.5194/acp-15-253-2015, 2015.

Chang, R. Y. W., Slowik, J. G., Shantz, N. C., Vlasenko, A., Liggio, J., Sjostedt, S. J., Leaitch, W. R., and Abbatt, J. P. D.: The hygroscopicity parameter (kappa) of ambient organic aerosol at a field site subject to biogenic and anthropogenic influences: relationship to degree of aerosol oxidation, Atmos. Chem. Phys., 10, 5047-5064, http://doi.org/10.5194/acp-10-5047-2010, 2010.

Cleveland, M. J., Ziemba, L. D., Griffin, R. J., Dibb, J. E., Anderson, C. H., Lefer, B., and Rappengluck, B.: Characterization of urban aerosol using aerosol mass spectrometry and proton nuclear magnetic resonance spectroscopy, Atmos. Environ., 54, 511-518, http://doi.org/10.1016/j.atmosenv.2012.02.074, 2012.

Cleveland, W. S. (1981) LOWESS: A program for smoothing scatterplots by robust locally weighted regression. Am. Stat., 35, 54.

Crippa, M., El Haddad, I., Slowik, J. G., DeCarlo, P. F., Mohr, C., Heringa, M. F., Chirico, R., Marchand, N., Sciare, J., Baltensperger, U., and Prevot, A. S. H.: Identification of marine and continental aerosol sources in Paris using high resolution aerosol mass spectrometry, J. Geophys. Res., 118, 1950-1963, http://doi.org/10.1002/jgrd.50151, 2013.

DeCarlo, P. F., Kimmel, J. R., Trimborn, A., Northway, M. J., Jayne, J. T., Aiken, A. C., Gonin, M., Fuhrer, K., Horvath, T., Docherty, K. S., Worsnop, D. R., and Jimenez, J. L.: Field-deployable, high-resolution, time-of-flight aerosol mass spectrometer, Anal. Chem., 78,

713 8281-8289, http://doi.org/10.1021/ac061249n, 2006.
714 Duplissy, J., DeCarlo, P. F., Dommen, J., Alfarra, M. R., Metzger, A., Barmpadimos, I., Prevot, A.
715 S. H., Weingartner, E., Tritscher, T., Gysel, M., Aiken, A. C., Jimenez, J. L., Canagaratna, M.
716 R., Worsnop, D. R., Collins, D. R., Tomlinson, J., and Baltensperger, U.: Relating
717 hygroscopicity and composition of organic aerosol particulate matter, Atmos. Chem. Phys.,
718 11, 1155-1165, http://doi.org/10.5194/acp-11-1155-2011, 2011.
719 El-Sayed, M. M. H., Amenumey, D., and Hennigan, C. J.: Drying-Induced Evaporation of
720 Secondary Organic Aerosol during Summer, Environ Sci Technol, 50, 3626-3633,
721 10.1021/acs.est.5b06002, 2016.
722 Ervens, B., Turpin, B. J., and Weber, R. J.: Secondary organic aerosol formation in cloud droplets
723 and aqueous particles (aqSOA): a review of laboratory, field and model studies, Atmos.
724 Chem. Phys., 11, 11069-11102, http://doi.org/10.5194/acp-11-11069-2011, 2011.
725 Farmer, D. K., Matsunaga, A., Docherty, K. S., Surratt, J. D., Seinfeld, J. H., Ziemann, P. J., and
726 Jimenez, J. L.: Response of an aerosol mass spectrometer to organonitrates and
727 organosulfates and implications for atmospheric chemistry, P. Natl. Acad. Sci. USA, 107,
728 6670-6675, http://doi.org/10.1073/pnas.0912340107, 2010.
729 Fountoukis, C., and Nenes, A.: ISORROPIA II: a computationally efficient thermodynamic
730 equilibrium model for K+-Ca2+-Mg2+-Nh(4)(+)-Na+-SO42--NO3--Cl--H2O aerosols,
731 Atmos. Chem. Phys., 7, 4639-4659, , http://doi.org/10.5194/acp-7-4639-2007, 2007.
732 Fry, J. L., Kiendler-Scharr, A., Rollins, A. W., Wooldridge, P. J., Brown, S. S., Fuchs, H., Dube,
733 W., Mensah, A., dal Maso, M., Tillmann, R., Dorn, H. P., Brauers, T., and Cohen, R. C.:
734 Organic nitrate and secondary organic aerosol yield from NO3 oxidation of beta-pinene
735 evaluated using a gas-phase kinetics/aerosol partitioning model, Atmos. Chem. Phys., 9,
736 1431-1449, http://doi.org/10.5194/acp-9-1431-2009, 2009.
737 Fry, J. L., Draper, D. C., Zarzana, K. J., Campuzano-Jost, P., Day, D. A., Jimenez, J. L., Brown, S.
738 S., Cohen, R. C., Kaser, L., Hansel, A., Cappellin, L., Karl, T., Roux, A. H., Turnipseed, A.,
739 Cantrell, C., Lefer, B. L., and Grossberg, N.: Observations of gas- and aerosol-phase organic
740 nitrates at BEACHON-RoMBAS 2011, Atmos. Chem. Phys., 13, 8585-8605,
741 http://doi.org/10.5194/acp-13-8585-2013, 2013.
742 Grantz, D. A., Garner, J. H. B., and Johnson, D. W.: Ecological effects of particulate matter,
743 Environ. Int., 29, 213-239, http://doi.org/10.1016/S0160-4120(02)00181-2, 2003.
744 Guo, H., Xu, L., Bougiatioti, A., Cerully, K. M., Capps, S. L., Hite, J. R., Carlton, A. G., Lee, S.
745 H., Bergin, M. H., Ng, N. L., Nenes, A., and Weber, R. J.: Fine-particle water and pH in the

746 southeastern United States, Atmos. Chem. Phys., 15, 5211-5228,
747 http://doi.org/10.5194/acp-15-5211-2015, 2015.
748 Haman, C. L., Lefer, B., and Morris, G. A.: Seasonal Variability in the Diurnal Evolution of the
749 Boundary Layer in a Near-Coastal Urban Environment, J. Atmos. Ocean Tech., 29,
750 697-710, , http://doi.org/10.1175/Jtech-D-11-00114.1, 2012.
751 Hayes, P. L., Ortega, A. M., Cubison, M. J., Froyd, K. D., Zhao, Y., Cliff, S. S., Hu, W. W.,
752 Toohey, D. W., Flynn, J. H., Lefer, B. L., Grossberg, N., Alvarez, S., Rappenglueck, B.,
753 Taylor, J. W., Allan, J. D., Holloway, J. S., Gilman, J. B., Kuster, W. C., De Gouw, J. A.,
754 Massoli, P., Zhang, X., Liu, J., Weber, R. J., Corrigan, A. L., Russell, L. M., Isaacman, G.,
755 Worton, D. R., Kreisberg, N. M., Goldstein, A. H., Thalman, R., Waxman, E. M., Volkamer,
756 R., Lin, Y. H., Surratt, J. D., Kleindienst, E., Offenberg, J. H., Dusanter, S., Griffith, S.,
757 Stevens, P. S., Brioude, J., Angevine, W. M., and Jimenez, J. L.: Organic aerosol
758 composition and sources in Pasadena, California, during the 2010 CalNex campaign, J.
759 Geophys. Res., 118, 9233-9257, http://doi.org/10.1002/jgrd.50530, 2013.
760 Hennigan, C. J., Bergin, M. H., Dibb, J. E., and Weber, R. J.: Enhanced secondary organic
761 aerosol formation due to water uptake by fine particles, Geophys. Res. Lett., 35, L18801,
762 http://doi.org/10.1029/2008gl035046, 2008.
763 Hu, W. W., Campuzano-Jost, P., Palm, B. B., Day, D. A., Ortega, A. M., Hayes, P. L., Krechmer,
764 J. E., Chen, Q., Kuwata, M., Liu, Y. J., de Sa, S. S., McKinney, K., Martin, S. T., Hu, M.,
765 Budisulistiorini, S. H., Riva, M., Surratt, J. D., St Clair, J. M., Isaacman-Van Wertz, G., Yee,
766 L. D., Goldstein, A. H., Carbone, S., Brito, J., Artaxo, P., de Gouw, J. A., Koss, A., Wisthaler,
767 A., Mikoviny, T., Karl, T., Kaser, L., Jud, W., Hansel, A., Docherty, K. S., Alexander, M. L.,
768 Robinson, N. H., Coe, H., Allan, J. D., Canagaratna, M. R., Paulot, F., and Jimenez, J. L.:
769 Characterization of a real-time tracer for isoprene epoxydiols-derived secondary organic
770 aerosol (IEPOX-SOA) from aerosol mass spectrometer measurements, Atmos. Chem. Phys.,
771 15, 11807-11833, http://doi.org/10.5194/acp-15-11807-2015, 2015.
772 Hu, W. W., Hu, M., Hu, W., Jimenez, J. L., Yuan, B., Chen, W. T., Wang, M., Wu, Y. S., Chen, C.,
773 Wang, Z. B., Peng, J. F., Zeng, L. M., and Shao, M.: Chemical composition, sources, and
774 aging process of submicron aerosols in Beijing: Contrast between summer and winter, J.
775 Geophys. Res., 121, 1955-1977, http://doi.org/10.1002/2015jd024020, 2016.
776 Jimenez, J. L., Canagaratna, M. R., Donahue, N. M., Prevot, A. S. H., Zhang, Q., Kroll, J. H.,
777 DeCarlo, P. F., Allan, J. D., Coe, H., Ng, N. L., Aiken, A. C., Docherty, K. S., Ulbrich, I. M.,
778 Grieshop, A. P., Robinson, A. L., Duplissy, J., Smith, J. D., Wilson, K. R., Lanz, V. A.,

Hueglin, C., Sun, Y. L., Tian, J., Laaksonen, A., Raatikainen, T., Rautiainen, J., Vaattovaara, P., Ehn, M., Kulmala, M., Tomlinson, J. M., Collins, D. R., Cubison, M. J., Dunlea, E. J., Huffman, J. A., Onasch, T. B., Alfarra, M. R., Williams, P. I., Bower, K., Kondo, Y., Schneider, J., Drewnick, F., Borrmann, S., Weimer, S., Demerjian, K., Salcedo, D., Cottrell, L., Griffin, R., Takami, A., Miyoshi, T., Hatakeyama, S., Shimono, A., Sun, J. Y., Zhang, Y. M., Dzepina, K., Kimmel, J. R., Sueper, D., Jayne, J. T., Herndon, S. C., Trimborn, A. M., Williams, L. R., Wood, E. C., Middlebrook, A. M., Kolb, C. E., Baltensperger, U., and Worsnop, D. R.: Evolution of Organic Aerosols in the Atmosphere, Science, 326, 1525-1529, http://doi.org/10.1126/science.1180353, 2009.

Kim, H., Zhang, Q., Bae, G. N., Kim, J. Y., and Lee, S. B.: Sources and atmospheric processing of winter aerosols in Seoul, Korea: insights from real-time measurements using a high-resolution aerosol mass spectrometer, Atmos. Chem. Phys., 17, 2009-2033, http://doi.org/10.5194/acp-17-2009-2017, 2017.

Kota, S. H., Park, C., Hale, M. C., Werner, N. D., Schade, G. W., and Ying, Q.: Estimation of VOC emission factors from flux measurements using a receptor model and footprint analysis, Atmos Environ, 82, 24-35, 10.1016/j.atmosenv.2013.09.052, 2014.

Kuwata, M., Zorn, S. R., and Martin, S. T.: Using Elemental Ratios to Predict the Density of Organic Material Composed of Carbon, Hydrogen, and Oxygen, Environ. Sci. Technol., 46, 787-794, http://doi.org/10.1021/es202525q, 2012.

Leong, Y. J., Sanchez, N. P., Wallace, H. W., Cevik, B. K., Hernandez, C. S., Han, Y., Flynn, J. H., Massoli, P., Floerchinger, C., Fortner, E. C., Herndon, S., Bean, J. K., Hildebrandt Ruiz, L., Jeon, W., Choi, Y., Lefer, B., and Griffin, R. J.: Overview of surface measurements and spatial characterization of submicrometer particulate matter during the DISCOVER-AQ 2013 campaign in Houston, TX, J. Air Waste Manage., 67, 854-872, http://doi.org/10.1080/10962247.2017.1296502, 2017.

Leuchner, M., and Rappengluck, B.: VOC source-receptor relationships in Houston during TexAQS-II, Atmos Environ, 44, 4056-4067, 10.1016/j.atmosenv.2009.02.029, 2010.

Li, J. Y., Cleveland, M., Ziemba, L. D., Griffin, R. J., Barsanti, K. C., Pankow, J. F., and Ying, Q.: Modeling regional secondary organic aerosol using the Master Chemical Mechanism, Atmos. Environ., 102, 52-61, http://doi.org/10.1016/j.atmosenv.2014.11.054, 2015.

Lim, Y. B., Tan, Y., Perri, M. J., Seitzinger, S. P., and Turpin, B. J.: Aqueous chemistry and its role in secondary organic aerosol (SOA) formation, Atmos. Chem. Phys., 10, 10521-10539, http://doi.org/10.5194/acp-10-10521-2010, 2010.

812 Liu, J. B., Rhland, K. M., Chen, J. H., Xu, Y. Y., Chen, S. Q., Chen, Q. M., Huang, W., Xu, Q. H.,
813 Chen, F. H., and Smol, J. P.: Aerosol-weakened summer monsoons decrease lake fertilization
814 on the Chinese Loess Plateau, Nat. Clim. Change, 7, 190-194, http://10.1038/Nclimate3220,
815 2017.
816 Mao, J. Q., Ren, X. R., Chen, S. A., Brune, W. H., Chen, Z., Martinez, M., Harder, H., Lefer, B.,
817 Rappengluck, B., Flynn, J., and Leuchner, M.: Atmospheric oxidation capacity in the
818 summer of Houston 2006: Comparison with summer measurements in other metropolitan
819 studies, Atmos. Environ., 44, 4107-4115, http://doi.org/10.1016/j.atmosenv.2009.01.013,
820 2010.
821 McKeen, S., Grell, G., Peckham, S., Wilczak, J., Djalalova, I., Hsie, E. Y., Frost, G., Peischl, J.,
822 Schwarz, J., Spackman, R., Holloway, J., de Gouw, J., Warneke, C., Gong, W., Bouchet, V.,
823 Gaudreault, S., Racine, J., McHenry, J., McQueen, J., Lee, P., Tang, Y., Carmichael, G. R.,
824 and Mathur, R.: An evaluation of real-time air quality forecasts and their urban emissions
825 over eastern Texas during the summer of 2006 Second Texas Air Quality Study field study, J.
826 Geophys. Res., 114, D00f11, http://doi.org/10.1029/2008JD011697, 2009.
827 Middlebrook, A. M., Bahreini, R., Jimenez, J. L., and Canagaratna, M. R.: Evaluation of
828 Composition-Dependent Collection Efficiencies for the Aerodyne Aerosol Mass
829 Spectrometer using Field Data, Aerosol Sci. Tech., 46, 258-271,
830 http://doi.org/10.1080/02786826.2011.620041, 2012.
831 Olaguer, E. P., Kolb, C. E., Lefer, B., Rappenglueck, B., Zhang, R. Y., and Pinto, J. P.: Overview
832 of the SHARP campaign: Motivation, design, and major outcomes, J. Geophys. Res., 119,
833 2597-2610, http://doi.org/10.1002/2013jd019730, 2014.
834 Paatero, P., Hopke, P. K., Song, X. H., and Ramadan, Z.: Understanding and controlling rotations
835 in factor analytic models, Chemometr. Intell. Lab, 60, 253-264,
836 http://doi.org/10.1016/S0169-7439(01)00200-3, 2002.
837 Paatero, P., and Tapper, U.: Positive matrix factorization: A non-negative factor model with
838 optimal utilization of error estimates of data values, Environmetrics, 5, 111-126,
839 https://doi.org/10.1002/env.3170050203, 1994.
840 Parrish, D. D., Allen, D. T., Bates, T. S., Estes, M., Fehsenfeld, F. C., Feingold, G., Ferrare, R.,
841 Hardesty, R. M., Meagher, J. F., Nielsen-Gammon, J. W., Pierce, R. B., Ryerson, T. B.,
842 Seinfeld, J. H., and Williams, E. J.: Overview of the Second Texas Air Quality Study
843 (TexAQS II) and the Gulf of Mexico Atmospheric Composition and Climate Study
844 (GoMACCS), J. Geophys. Res., 114, D00f13, http://doi.org/10.1029/2009jd011842, 2009.

Petters, M. D., and Kreidenweis, S. M.: A single parameter representation of hygroscopic growth and cloud condensation nucleus activity, Atmos. Chem. Phys., 7, 1961-1971, , http://doi.org/10.5194/acp-7-1961-2007, 2007.

Petters, M. D., Wex, H., Carrico, C. M., Hallbauer, E., Massling, A., McMeeking, G. R., Poulain, L., Wu, Z., Kreidenweis, S. M., and Stratmann, F.: Towards closing the gap between hygroscopic growth and activation for secondary organic aerosol - Part 2: Theoretical approaches, Atmos. Chem. Phys., 9, 3999-4009, http://doi.org/10.5194/acp-9-3999-2009, 2009.

Prenni, A. J., Petters, M. D., Kreidenweis, S. M., DeMott, P. J., and Ziemann, P. J.: Cloud droplet activation of secondary organic aerosol, J. Geophys. Res., 112, D10223, http://doi.org/10.1029/2006jd007963, 2007.

Racherla, P. N., and Adams, P. J.: Sensitivity of global tropospheric ozone and fine particulate matter concentrations to climate change, J. Geophys. Res., 111, https://doi.org/10.1029/2005JD006939, 2006.

Rollins, A. W., Smith, J. D., Wilson, K. R., and Cohen, R. C.: Real Time In Situ Detection of Organic Nitrates in Atmospheric Aerosols, Environ. Sci. Technol., 44, 5540-5545, http://doi.org/10.1021/es100926x, 2010.

Rollins, A. W., Browne, E. C., Min, K. E., Pusede, S. E., Wooldridge, P. J., Gentner, D. R., Goldstein, A. H., Liu, S., Day, D. A., Russell, L. M., and Cohen, R. C.: Evidence for NOx Control over Nighttime SOA Formation, Science, 337, 1210-1212, http://doi.org/10.1126/science.1221520, 2012.

Russell, L. M., Takahama, S., Liu, S., Hawkins, L. N., Covert, D. S., Quinn, P. K., and Bates, T. S.: Oxygenated fraction and mass of organic aerosol from direct emission and atmospheric processing measured on the R/V Ronald Brown during TEXAQS/GoMACCS 2006, J. Geophys. Res., 114, D00F05, http://doi.org/10.1029/2008JD011275, 2009.

Schulze, B. C., Wallace, H. W., Bui, A. T., Flynn, J. H., Erickson, M. H., Alvarez, S., Dai, Q., Usenko, S., Sheesley, R. J., and Griffin, R. J.: The impacts of regional shipping emissions on the chemical characteristics of coastal submicron aerosols near Houston, TX, Atmos. Chem. Phys., 18, 14217-14241, http://doi.org/10.5194/acp-18-14217-2018, 2018.

Setyan, A., Zhang, Q., Merkel, M., Knighton, W. B., Sun, Y., Song, C., Shilling, J. E., Onasch, T. B., Herndon, S. C., Worsnop, D. R., Fast, J. D., Zaveri, R. A., Berg, L. K., Wiedensohler, A., Flowers, B. A., Dubey, M. K., and Subramanian, R.: Characterization of submicron particles influenced by mixed biogenic and anthropogenic emissions using high-resolution aerosol

878 mass spectrometry: results from CARES, Atmos. Chem. Phys., 12, 8131-8156,
879 http://doi.org/10.5194/acp-12-8131-2012, 2012.
880 Sullivan, A. P., Hodas, N., Turpin, B. J., Skog, K., Keutsch, F. N., Gilardoni, S., Paglione, M.,
881 Rinaldi, M., Decesari, S., Facchini, M. C., Poulain, L., Herrmann, H., Wiedensohler, A.,
882 Nemitz, E., Twigg, M. M., and Collett Jr, J. L.: Evidence for ambient dark aqueous SOA
883 formation in the Po Valley, Italy, Atmos. Chem. Phys., 16, 8095-8108,
884 http://doi.org/10.5194/acp-16-8095-2016, 2016.
885 Sun, Y. L., Zhang, Q., Schwab, J. J., Demerjian, K. L., Chen, W. N., Bae, M. S., Hung, H. M.,
886 Hogrefe, O., Frank, B., Rattigan, O. V., and Lin, Y. C.: Characterization of the sources and
887 processes of organic and inorganic aerosols in New York city with a high-resolution
888 time-of-flight aerosol mass spectrometer, Atmos. Chem. Phys., 11, 1581-1602,
889 https://doi.org/10.5194/acp-11-1581-2011, 2011.
890 Sun, Y. L., Du, W., Fu, P. Q., Wang, Q. Q., Li, J., Ge, X. L., Zhang, Q., Zhu, C. M., Ren, L. J.,
891 Xu, W. Q., Zhao, J., Han, T. T., Worsnop, D. R., and Wang, Z. F.: Primary and secondary
892 aerosols in Beijing in winter: sources, variations and processes, Atmos. Chem. Phys., 16,
893 8309-8329, http://doi.org/10.5194/acp-16-8309-2016, 2016.
894 Surratt, J. D., Gomez-Gonzalez, Y., Chan, A. W. H., Vermeylen, R., Shahgholi, M., Kleindienst,
895 T. E., Edney, E. O., Offenberg, J. H., Lewandowski, M., Jaoui, M., Maenhaut, W., Claeys,
896 M., Flagan, R. C., and Seinfeld, J. H.: Organosulfate formation in biogenic secondary
897 organic aerosol, J. Phys. Chem. A, 112, 8345-8378, http://doi.org/10.1021/jp802310p, 2008.
898 Tai, A. P. K., Mickley, L. J., and Jacob, D. J.: Correlations between fine particulate matter
899 (PM2.5) and meteorological variables in the United States: Implications for the sensitivity of
900 PM2.5 to climate change, Atmos. Environ., 44, 3976-3984,
901 http://10.1016/j.atmosenv.2010.06.060, 2010.
902 Ulbrich, I. M., Canagaratna, M. R., Zhang, Q., Worsnop, D. R., and Jimenez, J. L.: Interpretation
903 of organic components from Positive Matrix Factorization of aerosol mass spectrometric
904 data, Atmos. Chem. Phys., 9, 2891-2918, https://doi.org/10.5194/acp-9-2891-2009, 2009.
905 Wallace, H. W., Sanchez, N. P., Flynn, J. H., Erickson, M. H., Lefer, B. L., and Griffin, R. J.:
906 Source apportionment of particulate matter and trace gases near a major refinery near the
907 Houston Ship Channel, Atmos. Environ., 173, 16-29,
908 https://doi.org/10.1016/j.atmosenv.2017.10.049, 2018.
909 Watson, J. G.: Visibility: Science and regulation, J. Air Waste Manage., 52, 628-713,
910 http://doi10.1080/10473289.2002.10470813, 2002.

Wood, E. C., Canagaratna, M. R., Herndon, S. C., Onasch, T. B., Kolb, C. E., Worsnop, D. R., Kroll, J. H., Knighton, W. B., Seila, R., Zavala, M., Molina, L. T., DeCarlo, P. F., Jimenez, J. L., Weinheimer, A. J., Knapp, D. J., Jobson, B. T., Stutz, J., Kuster, W. C., and Williams, E. J.: Investigation of the correlation between odd oxygen and secondary organic aerosol in Mexico City and Houston, Atmos. Chem. Phys., 10, 8947-8968, http://doi.org/10.5194/acp-10-8947-2010, 2010.

Xu, L., Suresh, S., Guo, H., Weber, R. J., and Ng, N. L.: Aerosol characterization over the southeastern United States using high-resolution aerosol mass spectrometry: spatial and seasonal variation of aerosol composition and sources with a focus on organic nitrates, Atmos. Chem. Phys., 15, 7307-7336, http://doi.org/10.5194/acp-15-7307-2015, 2015.

Xu, W. Q., Han, T. T., Du, W., Wang, Q. Q., Chen, C., Zhao, J., Zhang, Y. J., Li, J., Fu, P. Q., Wang, Z. F., Worsnop, D. R., and Sun, Y. L.: Effects of Aqueous-Phase and Photochemical Processing on Secondary Organic Aerosol Formation and Evolution in Beijing, China, Environ. Sci. Technol., 51, 762-770, http://doi.org/10.1021/acs.est.6b04498, 2017.

Ying, Q., Li, J. Y., and Kota, S. H.: Significant Contributions of Isoprene to Summertime Secondary Organic Aerosol in Eastern United States, Environ. Sci. Technol., 49, 7834-7842, http://doi.org/10.1021/acs.est.5b02514, 2015.

Zhang, Q., Jimenez, J. L., Canagaratna, M. R., Ulbrich, I. M., Ng, N. L., Worsnop, D. R., and Sun, Y. L.: Understanding atmospheric organic aerosols via factor analysis of aerosol mass spectrometry: a review, Anal. Bioanal. Chem., 401, 3045-3067, https://doi.org/10.1007/s00216-011-5355-y, 2011.

Zhang, Q. J., Beekmann, M., Freney, E., Sellegri, K., Pichon, J. M., Schwarzenboeck, A., Colomb, A., Bourrianne, T., Michoud, V., and Borbon, A.: Formation of secondary organic aerosol in the Paris pollution plume and its impact on surrounding regions, Atmos. Chem. Phys., 15, 13973-13992, http://doi.org/10.5194/acp-15-13973-2015, 2015.

Zhu, Q., He, L. Y., Huang, X. F., Cao, L. M., Gong, Z. H., Wang, C., Zhuang, X., and Hu, M.: Atmospheric aerosol compositions and sources at two national background sites in northern and southern China, Atmos. Chem. Phys., 16, 10283-10297, http://doi.org/10.5194/acp-16-10283-2016, 2016.

Table 1 Statistics of meteorological parameters, gas-phase pollutants, NR-PM_1 species, and PMF OA factors for the winter and summer campaigns at UHSL.

Variables		Season	Ave. value ± 1 SD	Minimum value	Maximum value
Meteorological parameters	Temp (˚C)	Winter	9.3 ± 6.0	0.7	25.9
		Summer	23.6 ± 3.8	12.2	33.1
	RH (%)	Winter	76 ± 18	23	99
		Summer	72 ± 19	21	98
	WS (m s^{-1})	Winter	2.1 ± 1.4	6.8×10^{-3}	9.4
		Summer	2.1 ± 1.2	9.0×10^{-3}	6.7
	Radiometer (W m^{-2})	Winter	0.6 ± 0.9	0.02	3.6
		Summer	1.1 ± 1.3	0.02	4.6
Gas-phase pollutants (ppb)	O_3	Winter	23.0 ± 12.6	0.12	53.0
		Summer	34.9 ± 15.3	0.02	75.9
	CO	Winter	238.7 ± 71.9	98.5	621.1
		Summer	168.3 ± 75.5	103.6	1110.2
	SO_2	Winter	1.0 ± 1.9	5.7×10^{-3}	29.5
		Summer	0.7 ± 1.7	2.8×10^{-3}	30.9
	NO	Winter	4.3 ± 6.4	2.0×10^{-3}	74.9
		Summer	1.3 ± 4.6	0.01	68.1
	NO_2	Winter	12.5 ± 9.7	0.8	101.2
		Summer	4.6 ± 6.4	0.2	44.4
	NO_y	Winter	22.9 ± 19.6	2.8	210.9
		Summer	8.6 ± 11.9	1.3	123.9
NR-PM_1 species (μg m^{-3})	OA	Winter	2.3 ± 1.4	0.42	9.4
		Summer	1.7 ± 1.4	0.27	12.3
	Sulfate	Winter	1.4 ± 0.8	0.05	3.4
		Summer	1.3 ± 0.6	0.02	5.6
	Nitrate	Winter	1.4 ± 1.4	0.02	6.9
		Summer	0.08 ± 0.1	0.01	0.9
	Ammonium	Winter	0.9 ± 0.6	BDL[a]	2.8
		Summer	0.5 ± 0.2	0.02	1.8
	Chloride	Winter	0.06 ± 0.09	BDL	1.1
		Summer	0.02 ± 0.02	BDL	0.5
OA factors (μg m^{-3})	HOA	Winter	0.3 ± 0.4	0[b]	8.6
		Summer	0.2 ± 0.5	0	10.9
	BBOA	Winter	0.6 ± 0.6	0	3.7
		Summer	0.1 ± 0.3	0	5.4
	COA	Winter	0.5 ± 0.5	0	4.8
	LO-OOA	Winter	0.4 ± 0.5	0	2.1
		Summer	0.7 ± 0.9	0	6.7
	MO-OOA	Winter	0.5 ± 0.3	0	1.8
		Summer	0.3 ± 0.2	0	1.6

[a]BDL: below detection limit; [b]Statistically determined factor concentrations with values below $1.0\text{x}10^{-3}$ are listed as 0.

945 **Table** 2 Correlation (*r*) of OOA mass spectra with previously published spectra database.
946 (http://cires1.colorado.edu/jimenez-group/HRAMSsd/)

Factor	Winter		Summer		Reference
	MO-OOA	LO-OOA	MO-OOA	LO-OOA	
aq-OOA[a]	**0.96**	0.75	**0.96**	**0.95**	Sun et al., 2016
MO-OOA	0.85	0.87	0.89	0.77	Setyan et al., 2012
MO-OOA	0.98	0.92	0.98	0.60	Hu et al., 2015
LV-OOA	0.97	0.91	0.98	0.62	Crippa et al., 2013
SV-OOA	0.65	0.70	0.70	0.78	Crippa et al., 2013
LO-OOAI, Biogenic-origin	0.83	0.84	0.86	0.76	Hu et al., 2015
LO-OOAII, Anthropogenic-origin	0.78	0.80	0.82	0.74	Hu et al., 2015

947 [a]aq-OOA is an aqueous-phase-processed SOA reported by Sun et al. (2016); LV=less volatile; SV=semi-volatile.

948

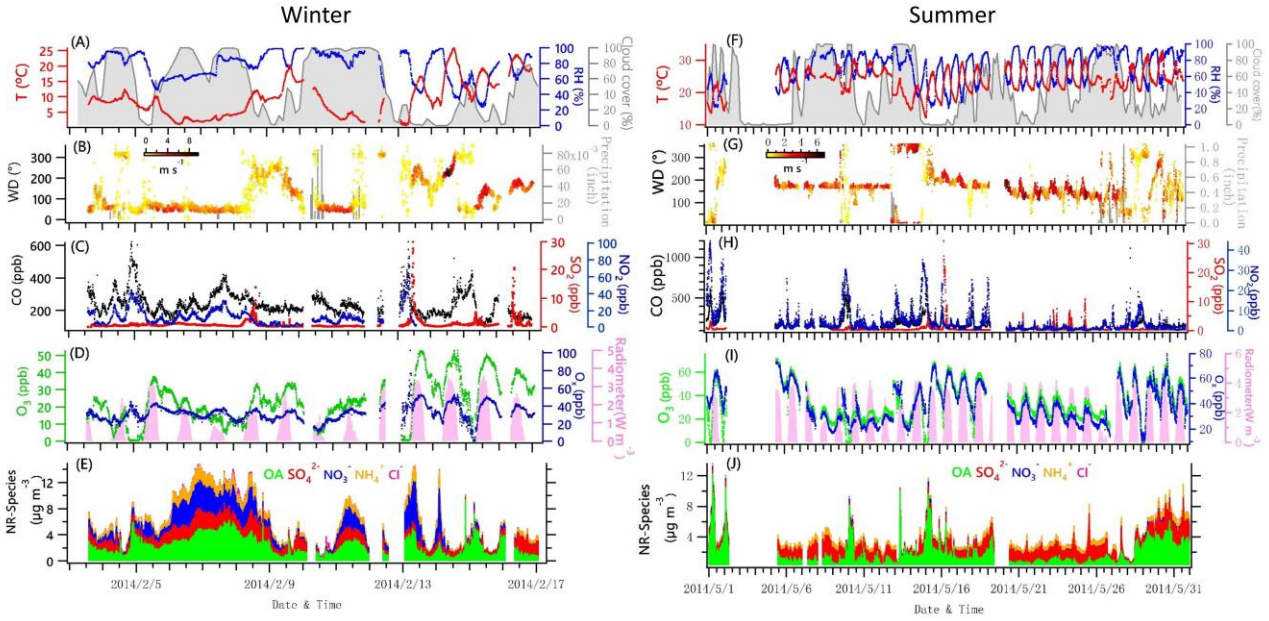

Figure 1. Time series of data collected at UHSL in Houston during the sampling periods in winter and summer 2014. Time series of 5-min average campaign data for **(A, F)** ambient temperature (T), relative humidity (RH) and total cloud cover (%, with 3 hours interval); **(B, G)** precipitation and wind direction (WD), with colors showing different wind speeds (WS); **(C, H)** CO, SO_2 and NO_2; **(D, I)** O_3, O_x (NO_2+O_3) and solar radiometer; **(E, J)** NR-PM_1 species, including OA, NO_3^-, SO_4^{2-}, NH_4^+, and Cl^-.

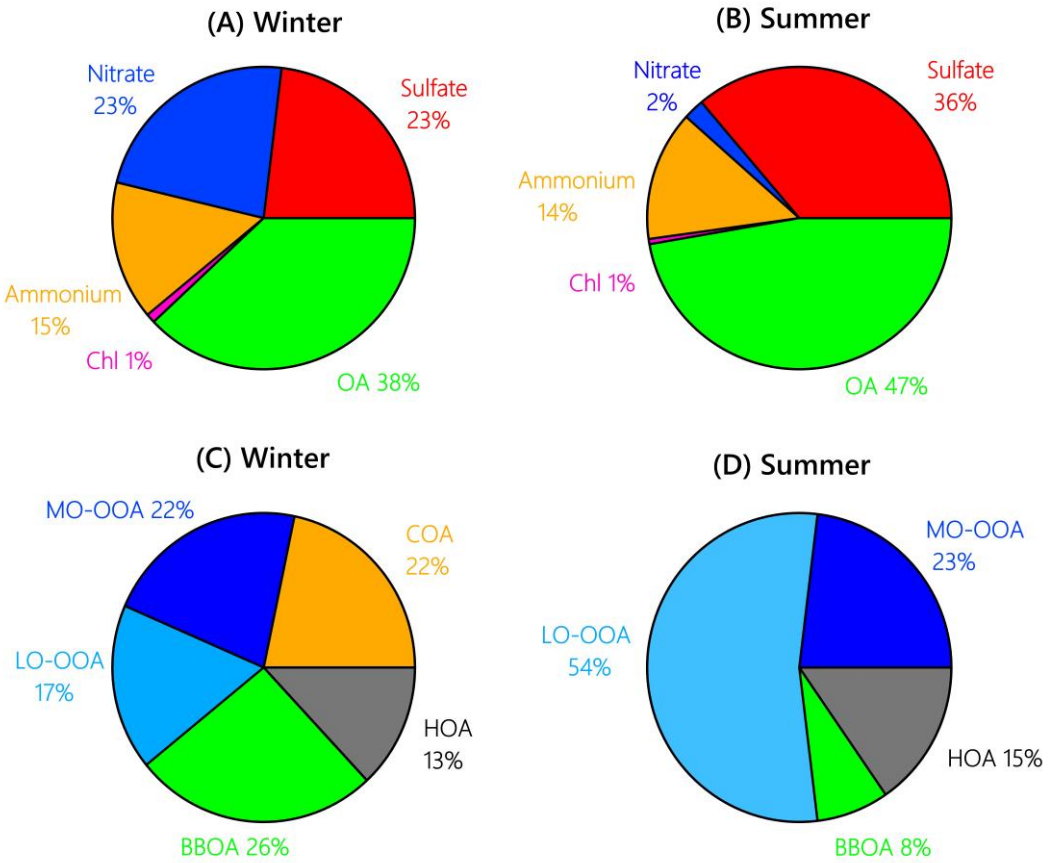

957

958 **Figure 2.** Average composition of NR-PM_1 species and OA factors during the winter (**A, C**) and
959 summer campaign (**B, D**) at UHSL.

960

961

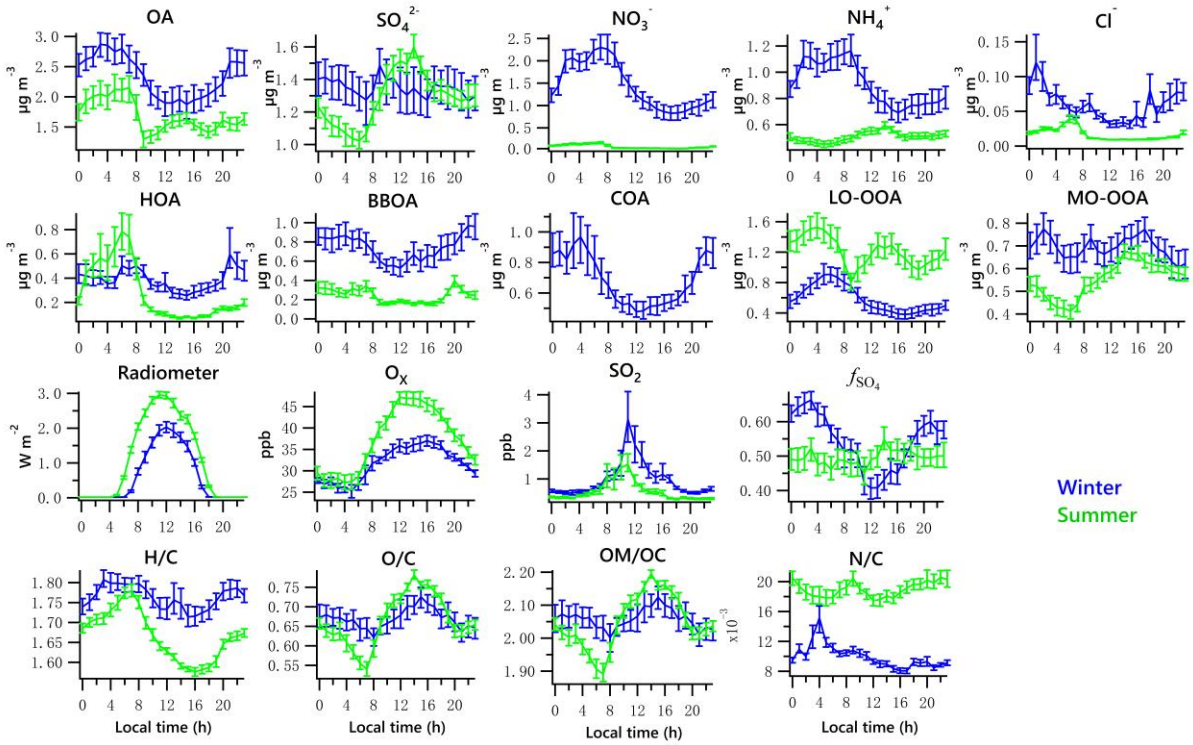

962

963 **Figure 3.** Diurnal profiles of the five NR-PM_1 species (OA, SO_4^{2-}, NO_3^-, NH_4^+ and Cl^-),
964 PMF-resolved factors (HOA, BBOA, COA, LO-OOA and MO-OOA), radiometer, O_x, SO_2, f_{SO4},
965 and elemental ratios (H/C, O/C, OM/OC and N/C). Lines denote the mean value, and bars
966 represent the 5/95 percent confidence interval in the mean (blue for winter, green for summer).

967

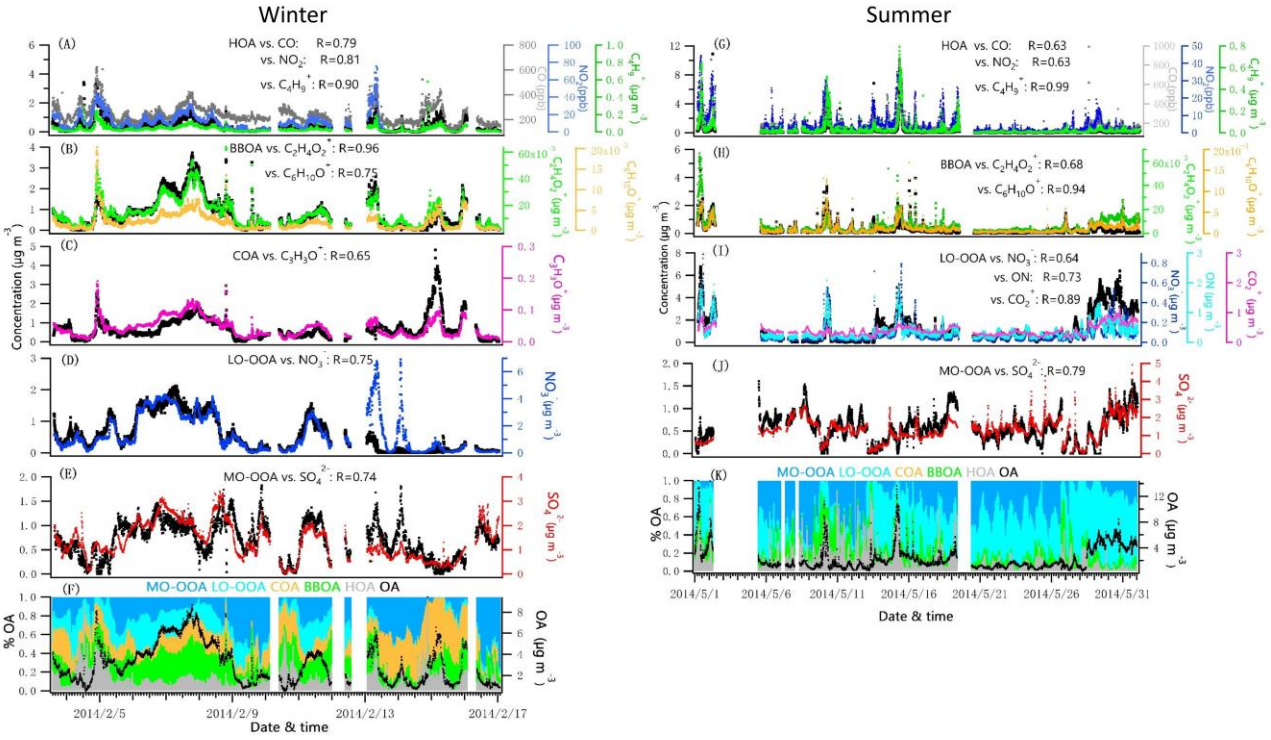

Figure 4. Time series of each OA factor and associated correlated species for the winter and summer campaign at UHSL.

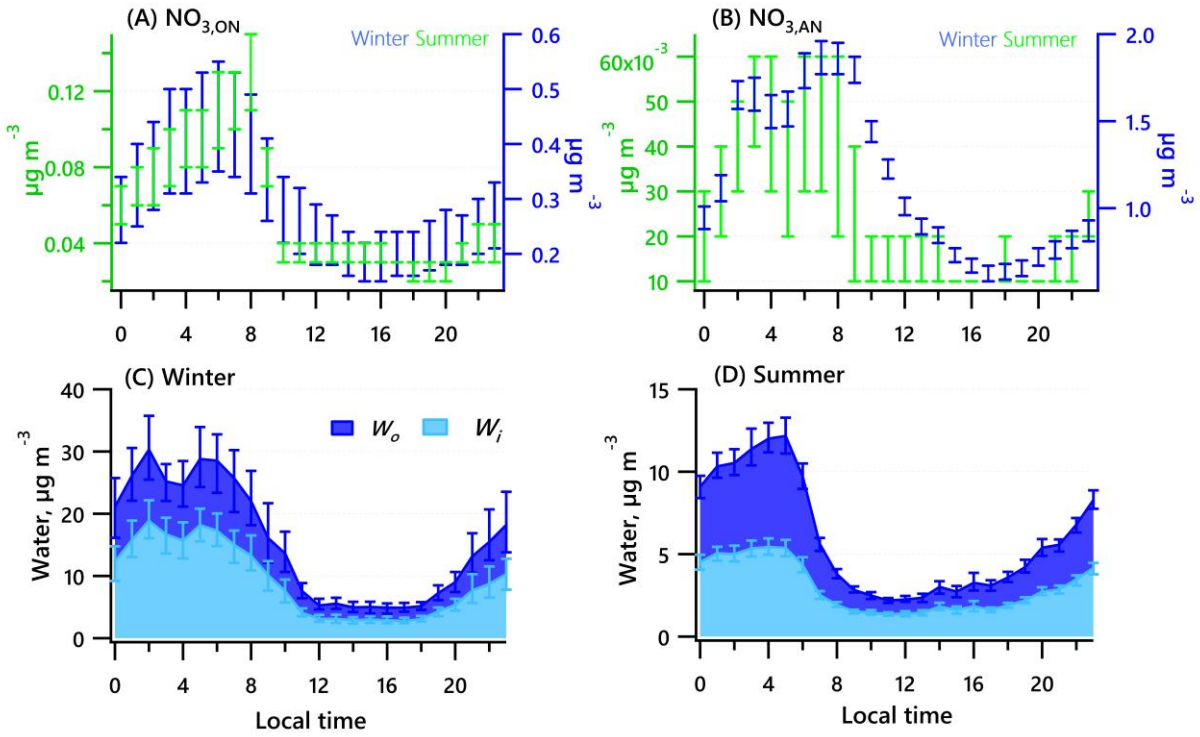

973

974 **Figure 5.** Diurnal profiles of the estimated range of nitrate functionality from organic nitrate (**A**)
975 and inorganic nitrate (**B**) for the winter and summer campaigns. Estimated water associated with
976 inorganic and organic aerosol for the winter (**C**) and summer campaigns (**D**). Solid lines denote
977 the mean value (blue for winter, green for summer), and bars represent the 5/95 percent
978 confidence interval in the mean.

979

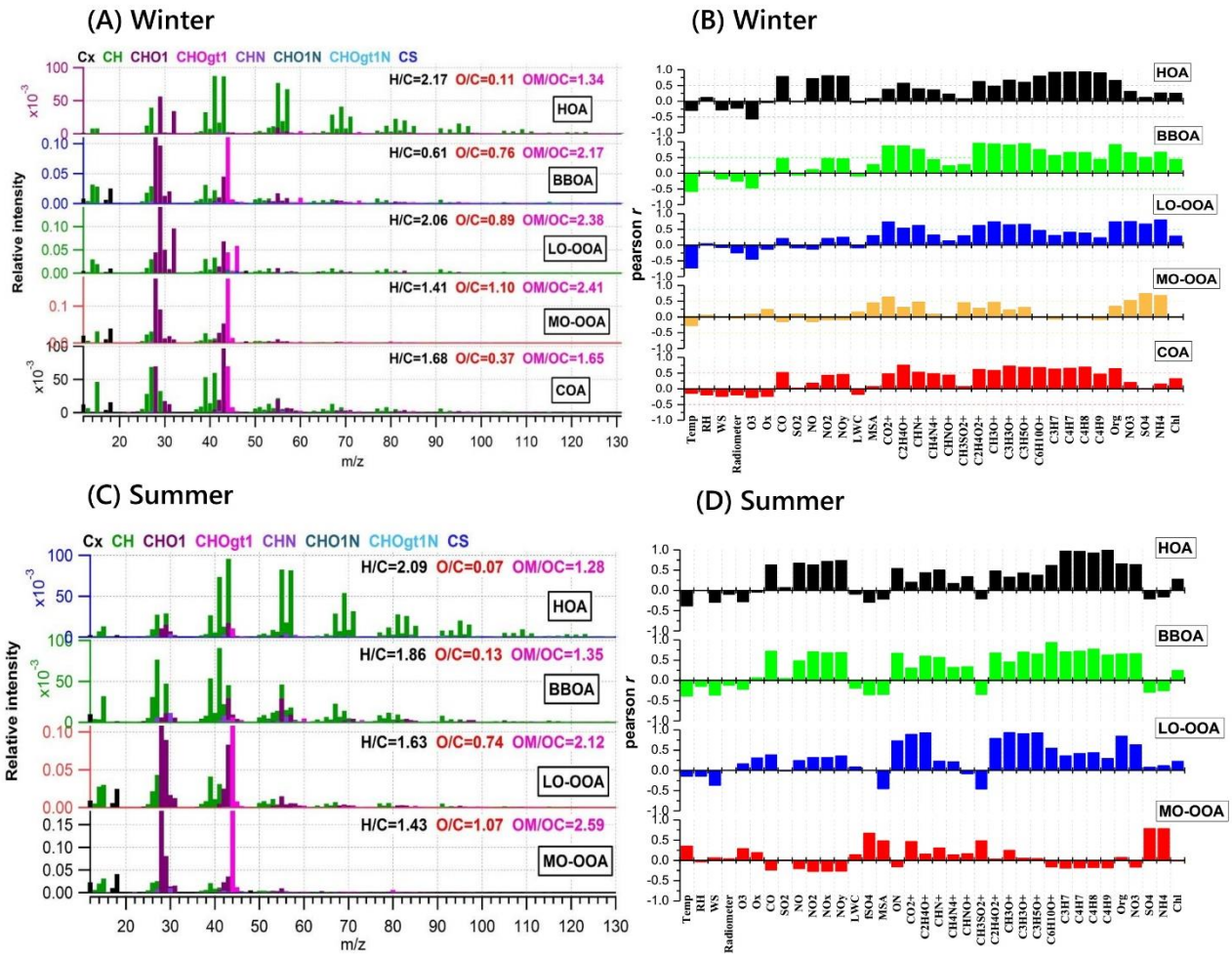

Figure 6. Mass spectra of PMF-resolved OA factors (**A**, **C**) and correlation coefficients between OA factors and other variables (tracer ions, trace gas, meteorological parameters, etc.) (**B**, **D**) for winter and summer campaigns at UHSL.

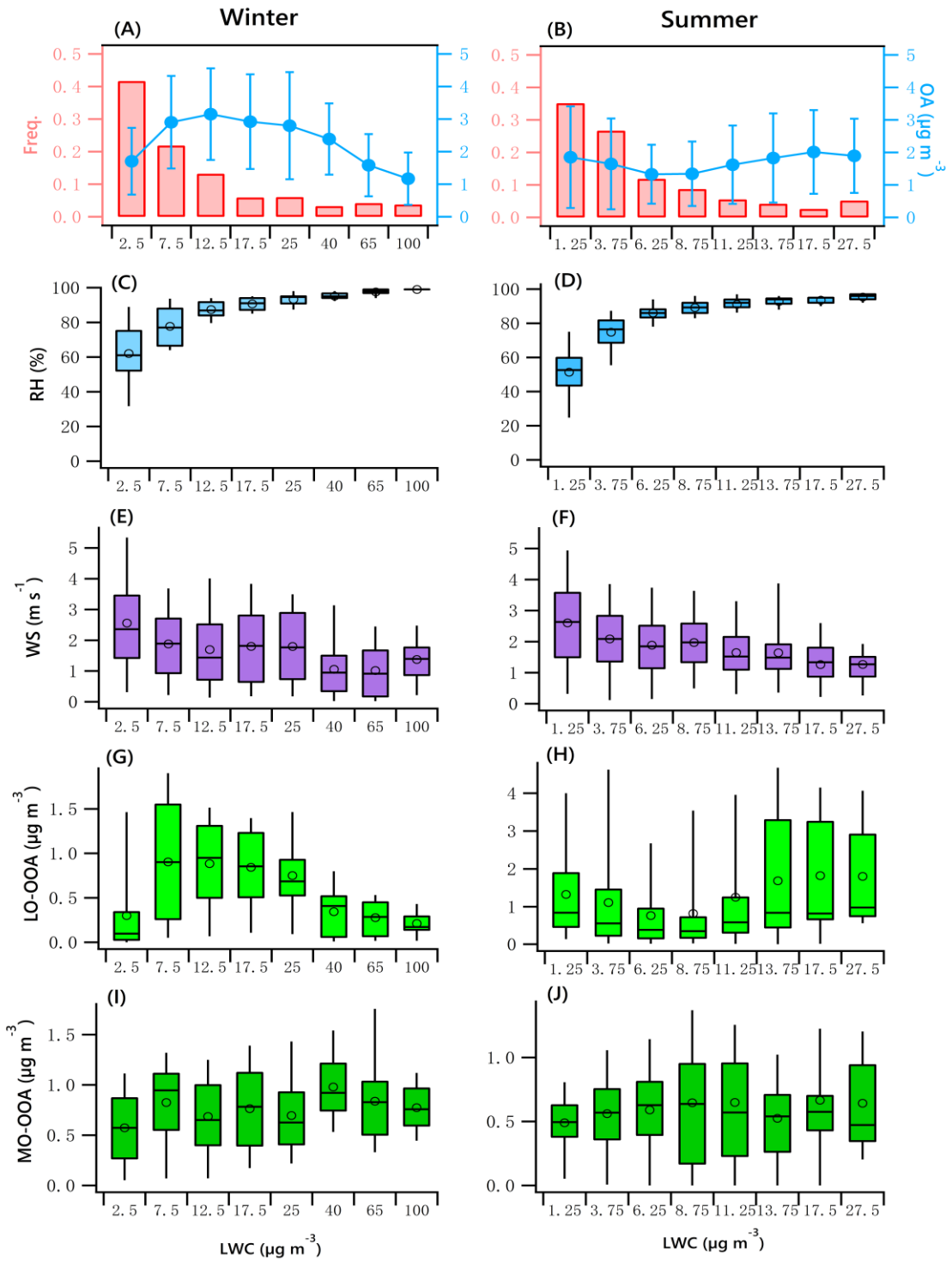

Figure 7. OA mass and frequency histograms of data points in each LWC bin for winter (**A**) and summer (**B**). Variations of RH, WS, LO-OOA and MO-OOA mass as a function of LWC in winter (**C, E, G, I**) and summer (**D, F, H, J**). The data were binned according to the LWC (with different increment values), and mean (circle), median (horizontal line), 25th and 75th percentiles (lower and upper box), and 5th and 95th percentiles (lower and upper whiskers) are displayed for data in each bin.

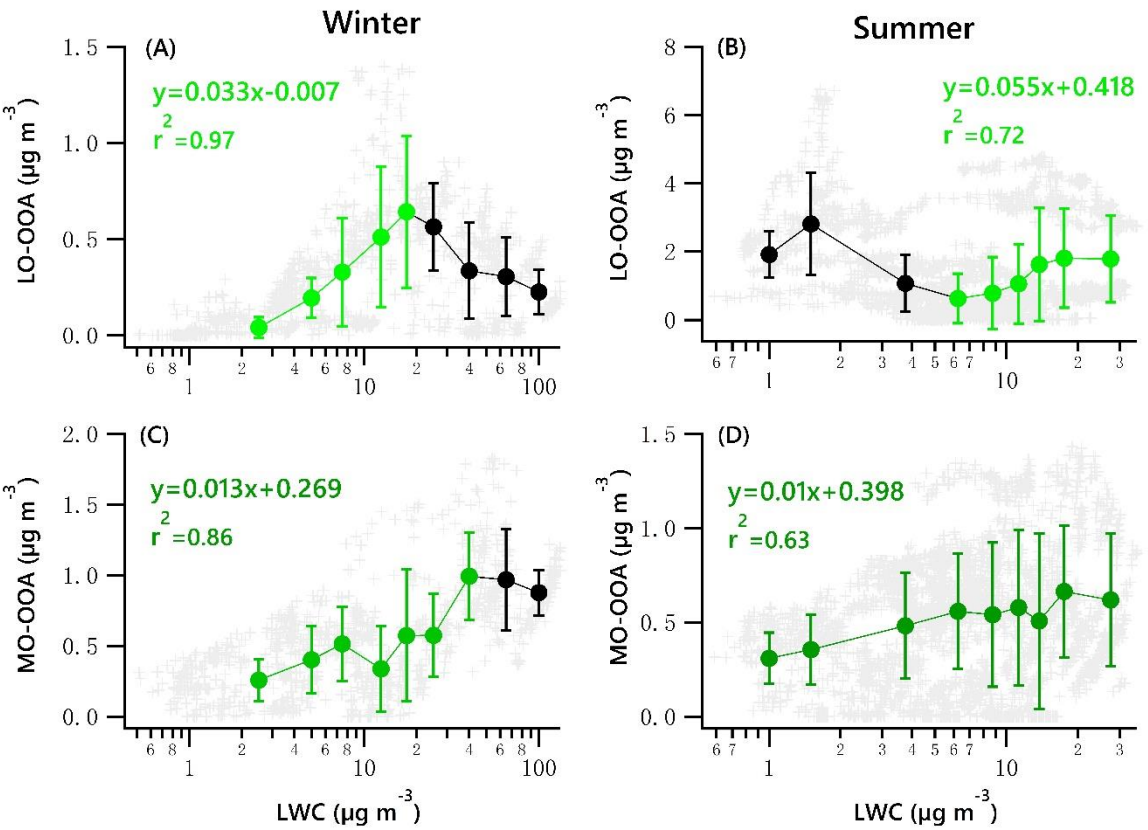

Figure 8. Scatter plots of nighttime OOA vs. LWC for the winter and summer campaign. The linear equations are given for fitting only the green dots. Solid dots denote the average value of data in each bin. Bars indicate standard deviations.

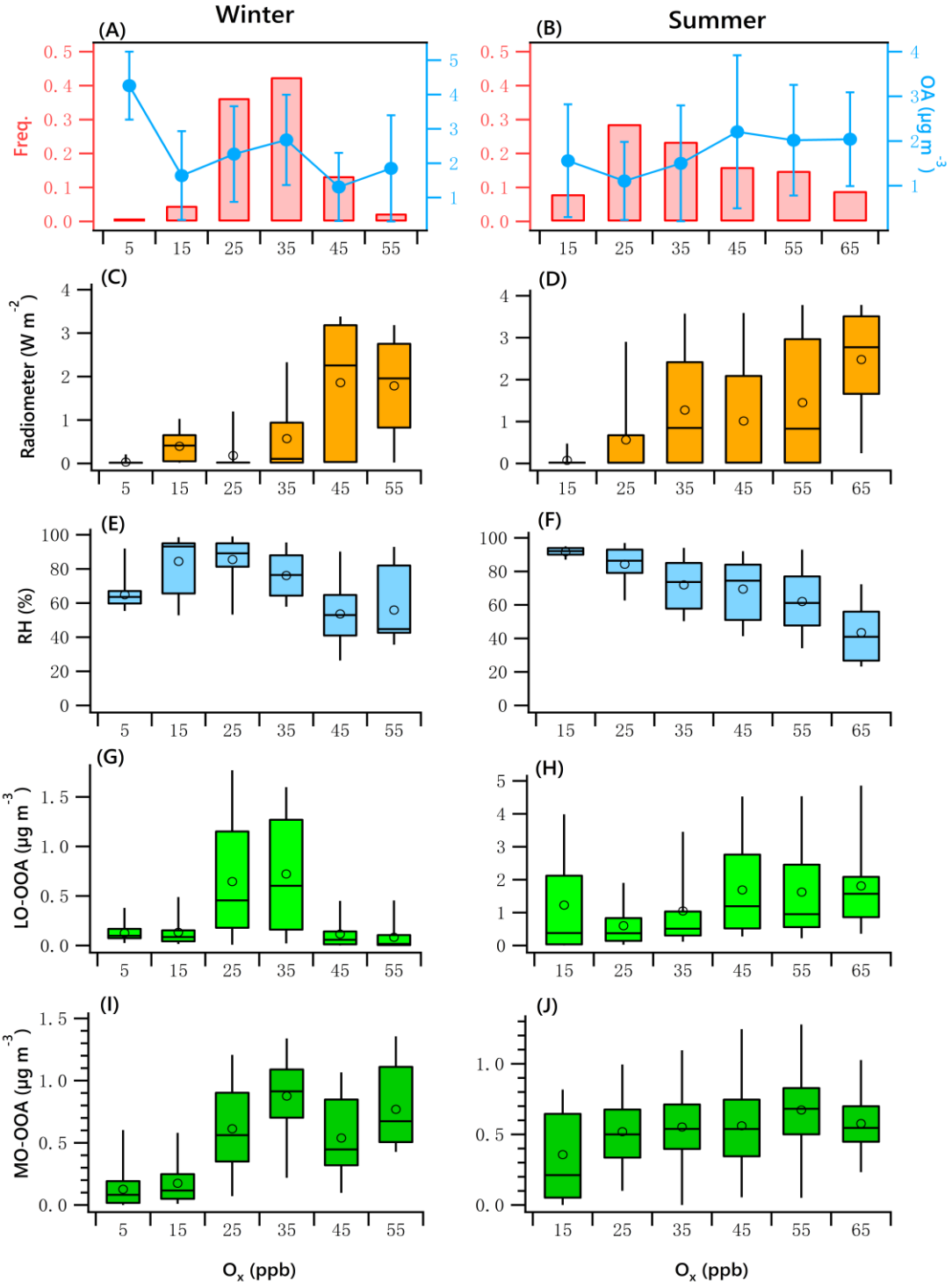

Figure 9. OA mass and frequency histograms of data points in each O_x bin for winter (**A**) and summer (**B**). Variations of solar radiation, RH, LO-OOA and MO-OOA mass as a function of LWC in winter (**C, E, G, I**) and summer (**D, F, H, J**). The data were binned according to the O_x (10 ppb increment), and mean (circle), median (horizontal line), 25th and 75th percentiles (lower and upper box), and 5th and 95th percentiles (lower and upper whiskers) are displayed for data in each bin.

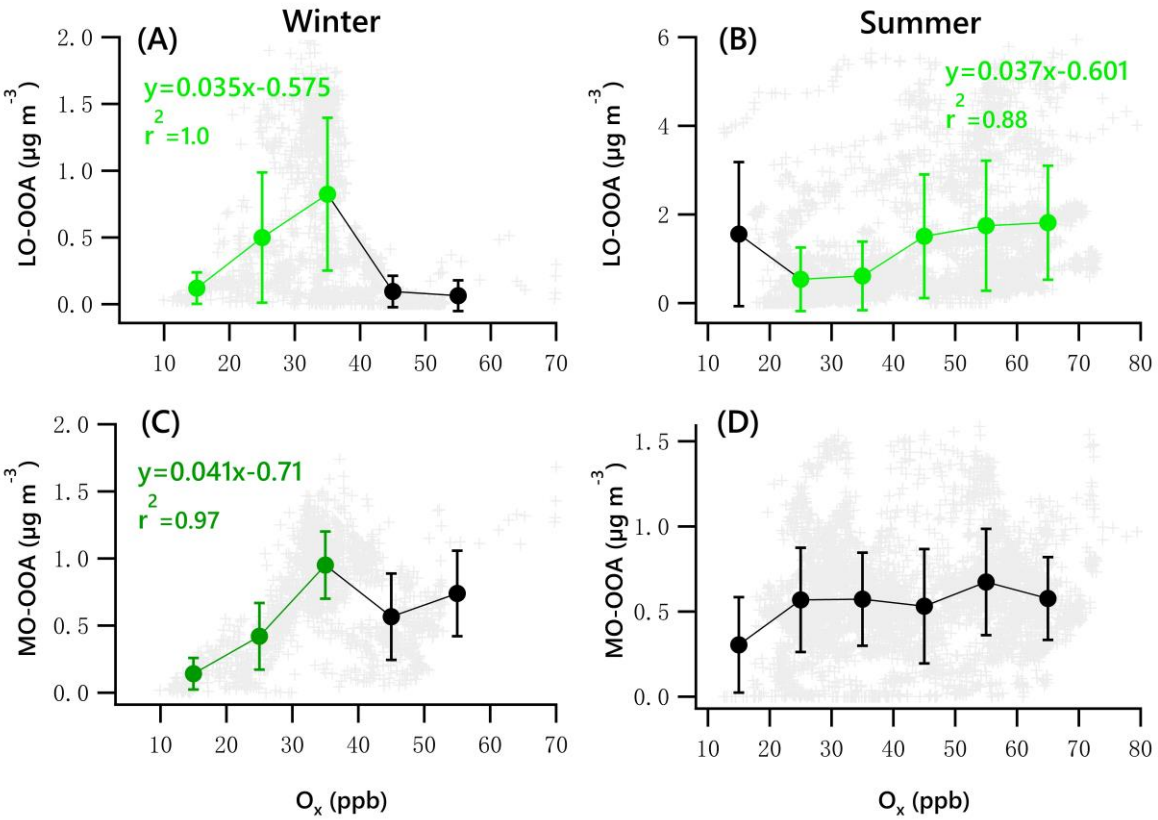

Figure 10. Scatter plots of daytime OOA vs. O_x for the winter and summer campaign. The linear equations are given for fitting the green dots. Bars indicate standard deviations.

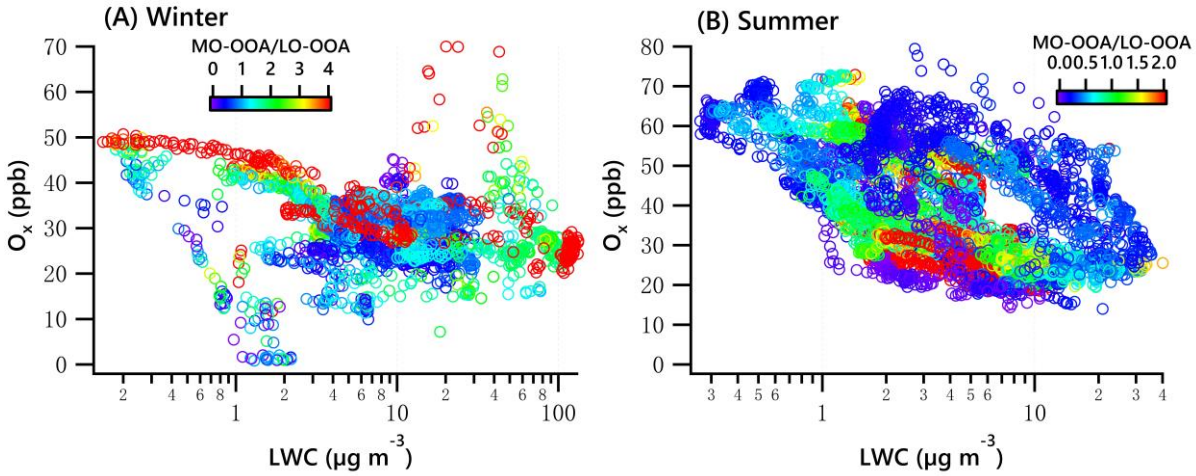

Figure 11. O_x vs LWC dependence of the ratio of MO-OOA/LO-OOA in winter (**A**) and summer (**B**).